DEPARTMENT OF THE INTERIOR
U.S. GEOLOGICAL SURVEY

Field guide to Proterozoic geology of the New York, Ivanpah, and Providence Mountains, California

Field Conference 1
Proterozoic Orogenesis and Metallogenesis Project

David M. Miller and Joseph L. Wooden
Menlo Park, CA 94025

U.S. Geological Survey
Open-File Report 94-674

INTRODUCTION

Early Proterozoic rocks form much of the continental crust of the Mojave Desert crustal province of southeastern California. A knowledge of these rocks and their origins is essential for understanding the Proterozoic and Phanerozoic evolution of the region. Early Proterozoic rocks in the Mojave Desert typically crop out as isolated small exposures within extensive tracts of Mesozoic granitoids; however, in the New York and McCullough Mountains and in much of the Ivanpah Mountains and contiguous Clark Mountain Range (Fig. 1), these rocks lie northeast of Mesozoic batholiths. Rocks in these mountain ranges offer the most complete view of Proterozoic geology in California.

Along with colleagues, we have studied the Early Proterozoic rocks in the northeastern part of the Mojave Desert for much of the past decade. Our work builds on the pioneering studies of Hewett (1956), who identified Precambrian metamorphic and igneous rocks, and described their relations with adjoining rocks. DeWitt and others (1984) dated gneissic granites in the Halloran Hills to the west (Fig. 1) as about 1.71 Ga, setting the stage for ensuing documentation of a granulite facies metamorphic event (the Ivanpah orogeny) along with pre-, syn-, and post-metamorphic granitoids (Wooden and Miller, 1990). Plutonic rocks from 1.76 to 1.66 Ga are now documented and some of their wallrocks contain zircons 700 m.y. older than the oldest granitoids. The emerging picture is one of a ~1.8 Ga sedimentary and volcanic province that in part received detritus from much older sources and (or) was built upon ~2.5 Ga basement. Rocks of this province were intruded, and perhaps deformed and metamorphosed, at 1.76 and ~1.73 Ga; magmas were mafic and metaluminous in some cases and K-rich in others. Between 1.71 and 1.695 Ga, a major orogenic event, the Ivanpah orogeny, thoroughly migmatized older rocks as well as synkinematic K-rich granitoids. The signature of the event is widespread migmatite that in many places is characterized by abundant leucocratic granitoids layers and by ubiquitous garnet. Metamorphism was at low pressure granulite facies (Thomas and others, 1988; Young, 1989; Young and others, 1989) in this region, and at higher pressure upper amphibolite facies southward in the Old Woman Mountains area (Foster and others, 1992). Following the Ivanpah orogeny, granitoids were emplaced in a north-south zone in the New York and McCullough Mountains from about 1.695 to 1.675 Ga (the New York Mountains intrusive suite). Following the emplacement of the New York Mountains intrusive suite, but overlapping some in time, granitoids such as the Big Tiger suite, Fenner Gneiss (Bender and others, 1990), and related rocks were emplaced throughout a somewhat wider region until about 1.66 Ga. Groups of plutons emplaced during these plutonic events were of batholithic dimensions and display an evolution from peraluminous K-rich magmas to metaluminous calc-alkaline magmas. Events since the youngest Early Proterozoic magmatism at 1.66 Ga are sketchy, but include: (1) formation of mylonite belts, perhaps during prolonged cooling through the Early and Middle Proterozoic, (2) ~1.4 Ga anorogenic magmatism, and (3) ~1.1 Ga diabase sheet intrusion.

High-grade rocks of the northeastern Mojave Desert appear to grade eastward, through the Cerbat and Hualapai Mountains of Arizona, to broad exposures of amphibolite and greenschist facies rocks within mountains bordering the Colorado Plateau (Karlstrom and Bowring, 1988). In fact, the New York Mountains lay considerably closer to the Cerbat Mountains prior to Miocene extension in the Colorado River region; about 90 km of extension is documented farther south (Spencer and Reynolds, 1991) and a large amount of extension may have taken place east of the New York Mountains. Ages of specific depositional, deformational, and plutonic events vary from block to block in these Arizona rocks, and debate has focused on whether they represent slightly shifted once-contiguous blocks or far-traveled allochthonous terranes. A fundamental isotopic boundary, recognized on the basis of Pb and Nd isotopic characteristics, lies in western Arizona (Bennett and DePaolo, 1987; Wooden and others, 1988; Wooden and Miller, 1990; Wooden and DeWitt, 1991) and is commonly taken as a boundary between two crustal provinces. Wooden and DeWitt (1991) showed that the two crustal provinces were contiguous by about 1.74 Ga, and therefore subsequent orogenic events in the Mojave crustal province must be integrated with the histories of tectonic blocks in the Arizona crustal province to arrive at a complete picture of Proterozoic orogenesis of the southwestern United States.

This report describes key field localities where Proterozoic lithologic sequences and intrusive relations are well exposed in the Ivanpah and New York Mountains. At many of these localities we integrate an extensive chronologic and geochemical data base with field relations (although only a small percentage of the analyses are given in tables). We expect users of this report to be familiar with the overview of Early Proterozoic geology given by Wooden and Miller (1990); we will describe localities and interpret them within that framework. Day 1, Stop 1 is a long traverse of spectacular dry stream bed exposures of early intrusive rocks and metamorphosed supracrustal rocks in the Ivanpah Mountains. For those unable to hike the rough 5- to 6-mile route, the nearby rocks can be studied and rocks representative of the remote part of the traverse can instead be seen easily at Optional Stops 1 and 2. On Day 2 we examine typical metamorphosed supracrustal and post-orogenic granitoid rocks of the northern New York Mountains. On Day 3 we examine more post-orogenic granitoid rocks in the New York Mountains and a large synorogenic plutonic complex in the northern Providence Mountains. For field trip participants interested in the Phanerozoic geology of the Ivanpah Valley region, Miller and others (1991) recently compiled much new data and provided an up-to-date list of references.

DAY 1

Cumulative Mileage

0.0 Begin at the Nipton Road exit off Interstate 15 in California, between Mountain Pass and the Nevada border (Figure 1). Drive east on Nipton Road.

3.3 Turn right on Ivanpah Road.

4.4 Turn right on poorly marked jeep track.

4.5 Stay to right and continue across abandoned air strip, turning directly toward mountain front to west.

5.8 STOP 1. Park on the road. We will take a several mile hike from here involving steep climbs on rocky slopes. Figure 2 portrays the geology and trip route (dashed line).

This structural section of the Ivanpah Mountains contains good exposures of generally pelitic and greywacke composition gneisses that are intruded by gabbro, quartz diorite, mafic granodiorite, and trondhjemitic rocks. All of these rocks are intruded by amphibolite dikes, which in turn predate or accompany the Ivanpah orogeny (1.705 Ga). From east to west, we will traverse several lithologic groups: (1) Metagabbro, (2) Meta-quartz diorite about 1.76 Ga, (3) Biotite-rich granodiorite gneiss about 1.76 Ga, (4) Pelitic gneiss intruded by various dikes, (5) Trondhjemitic gneisses forming wide dikes, sheets, or elongate plutons, and (6) Pelitic gneiss cut by numerous amphibolite bodies. These lithologic groups are strictly gradational in almost all cases, although margins of a few of the plutonic rock types can be closely delineated. All of these rocks are Early Proterozoic, as indicated by U-Pb study of zircon and by metamorphic and deformational relations similar to other rocks that experienced the ~1.705 Ga Ivanpah orogeny. High-angle faults that cut the Early Proterozoic rocks strike northwest and north-northwest and are nearly vertical. These faults displace rocks by some combination of dextral strike-slip and down-to-the-west offset. The faults commonly are the locus of dikes composed of shonkinite and carbonate, probably related to the nearby ~1.4 Ga Mountain Pass complex (DeWitt and others, 1987), and therefore probably first formed between 1.705 and 1.4 Ga. However, the ~1.4 Ga rocks are highly fractured, suggesting one or more episodes of fault reactivation.

(1) Examine the two black hills away from the range front. Outcrops are metagabbro, sparsely porphyritic (plagioclase phenocrysts), in which original igneous textures are preserved as polygonized groups of medium-grained minerals. The rock now has a granulite texture. The metagabbro is a plagioclase-clinopyroxene-orthopyroxene rock; chemically it is an aluminous gabbro with ~51% SiO_2 (see one analysis in Table 1). Biotite is present in the metagabbro along the east edge of the exposure, perhaps as a replacement of hornblende. In most places the metagabbro is separated from the dated meta-quartz diorite rocks in the range front by a septum of variably mylonitized pelitic gneiss, and locally it is retrograded to biotite-bearing rock. Because the pelitic gneiss is roughly 1.8 Ga on the basis of detrital zircons and is

probably intruded by gabbro, this metagabbro is between 1.8 and 1.7 Ga. We suggest that its age is close to that for the meta-quartz diorite (1.76 Ga) because its exposures are restricted to sites adjacent to, and it locally intrudes, the meta-quartz diorite.

(2) Proceed southwest across a saddle of inter-sheared gabbro, pelitic gneiss, and meta-quartz diorite. Continue up the steep hillside to the southwest. Where metagabbro is in contact with meta-quartz diorite on a small hill to the south, the contact is sharp but deformed. Intrusive relations are not proven. Meta-quartz diorite is a coarse-grained, biotite-rich rock with up to 10% K-spar megacrysts and is dated at about 1756 ± 19 Ma by U-Pb zircon techniques (Figure 3). Meta-quartz diorite ranges from 56 to 59% SiO_2 and has about 1-2% K_2O (Table 1, Figure 4), and chemically is a quartz diorite or calc-alkalic diorite. Leucocratic phases are felsic granite (unit Xl on map, Figure 2) and form pods up to 20 x 800 m. The meta-quartz diorite is also cut by leucocratic pegmatite dikes. The meta-quartz diorite is unique in being the oldest dated plutonic body in the Mojave province and in having an unusually mafic and calcic composition for that province.

Meta-quartz diorite is cut by amphibolite dikes of basaltic and ultramafic composition (Table 2), proving that some, and perhaps all, amphibolite is intrusive, rather than extrusive. Most amphibolites are chemically distinct from the metagabbro in that they are 44 to 50% SiO_2 and 10 to 20% MgO (Table 2), but some overlap in plots of major elements is apparent (Fig. 5). Amphibolites can be divided into high-Mg ultramafic rocks and rocks with tholeiitic chemistry (Fig. 5). Tholeiites can be further divided on the basis of Al content. Chemistry does not change with location; all types are represented in the Ivanpah Valley region.

Narrow mylonite zones in places border pegmatite dikes; these strike N 10 E and dip about 45 degrees west, and have down-to-the-west sense of separation (~10 m) where they cut amphibolite dikes that strike ~N 30 W and vertical.

Watch for dikes of brown shonkinite and orange carbonate related to the ~1.4 Ga Mountain Pass system; they commonly lie near and are involved within northwest-striking high-angle faults.

(3) Biotite-rich granodiorite gneisses constitute a heterogeneous group of rocks making up a thick structural section (units Xbg and Xag, Fig. 2). The hallmark of these gneisses is a large amount (60-80%) of metaigneous rock, much of which is biotite-rich granodiorite in composition. The gneisses now form 1- to 5-m thick layers and show textural and compositional variability from fine-medium grained biotite-rich gneiss with 61 to 64% SiO_2 to medium-coarse grained porphyritic augen gneiss (unit Xag) with 5% biotite and 66 to 67% SiO_2. The finer grained biotite-rich rocks appear to form two compositional groups, although the distinction is not clear in Fig. 4 because most of the analyses are for porphyritic rocks. Group one is 66 to 69% SiO_2, 2% total Fe, and high Ca (3 to 4%) and Na_2O (4 to 5%) compared to K_2O (1 to 2%). Group two has lower SiO_2 (61 to 64%) and is iron and K_2O rich (7 to 8%, 3 to 4%). Both groups are weakly peraluminous and moderately sodic. Porphyritic rocks (Fig. 4) have SiO_2 similar to group one (66 to 67%), but higher Fe (4 to 5%) and subequal CaO, Na_2O and K_2O (2 to 4%, 2 to 3%, 2 to 6%). Porphyritic rocks are abundant in a linear zone, distinguished on Figure 2 as an augen gneiss (Xag) unit. Where relatively undeformed 1 km to the south (Optional Stop 1), the rock is clearly igneous on the basis of texture and homogeneity. There, augen gneiss grades into finer grained biotite-rich granodiorite and rock very similar to the meta-quartz diorite, suggesting these three phases have temporally related igneous origins. Discordant zircons from the augen gneiss at Optional Stop 1 are co-linear with zircons from the meta-quartz diorite unit (Fig. 3), further supporting related igneous origins.

Interlayered with the biotite-rich granodioritic gneisses are pelitic gneiss, amphibolite, leucocratic dikes, biotite-garnet gneiss, and rare gabbro dikes. The total assemblage shows no consistent compositional change westward that we have identified. The biotite-rich granodioritic gneisses are most easily distinguished from rocks in previously examined lithologic groups by abundant garnet, and from upcoming lithologic groups by abundance of metaigneous textures and compositions. Amphibolite and gabbro in the biotite-rich granodiorite group are similar to those previously described.

We consider the granodiorite gneisses to be of igneous origin because they contain K-spar and plagioclase of varying sizes, many as single crystals, as though they were originally phenocrysts. Metamorphism of a sedimentary or fine-grained volcanic rock is unlikely to produce this texture. In places, the granodiorite gneiss contains K-spar augen up to 2 cm long, which seems to require an intrusive origin. The more biotite-rich granodiorite has an igneous composition (Table 1), but we cannot rule out a weathering role or a sedimentary mixing of volcanic rocks and minor clays for its origin. Indeed, analyses for some rocks with igneous-looking texture (not in Table 1) suggest that they must be modified from an igneous protolith, for they are exceptionally aluminous.

The compositional variation within the granodiorite gneiss group suggests some combination of numerous small bodies or dikes of plutonic rocks, and (or) crystal-rich volcanic flows, along with shale-rich sedimentary rock and graywacke or (and) reworked volcanic rock. We envision a heavily intruded group of immature sediment as a likely model for the rocks. The extent to which deformation and metamorphism contributed to the heterogeneous nature of this group is not resolvable. In contrast, meta-quartz diorite is much less intermixed with other gneiss, which may be due to: (1) meta-quartz diorite was intruded after part of the strain caused mixing in the granodiorite group; (2) meta-quartz diorite is a drier, probably stiffer, rock type; and (3) meta-quartz diorite intruded as a large pluton, whereas intrusive bodies in the granodiorite gneiss group were much smaller. If option (1) is true, meta-quartz diorite is younger than igneous rocks of the biotite granodiorite gneiss group. At a minimum, we consider by the spatial proximity of the quartz diorite and rocks of the biotite granodiorite gneiss group that they have comparable ages. U-Pb studies to test these hypotheses are in progress.

Southward in the Ivanpah Mountains and along strike with the biotite granodiorite gneiss group, rocks with igneous compositions different from those we encounter on this traverse are abundant. The distinctive gneisses consist of hornblende-bearing meta-granodiorite and related sodic gneisses. These sodic gneisses (Fig. 4, Table 1) are compositionally intermediate between rocks of the granodiorite gneiss and the meta-quartz diorite in many respects.

(4) The pelitic gneiss lithologic group consists of pelitic (biotite-sillimanite) gneiss, semi-pelitic (biotite-rich) gneiss, and biotite-garnet gneiss, along with varied leucocratic dikes, compose most of the rock west of the biotite-rich granodiorite gneiss lithologic group. Demonstrably igneous rocks are minor, although light-gray biotite gneiss with distinctive paw-print clusters of garnet localized along leucocratic veins may be an exception (paw-print gneiss, Table 1). Biotite-garnet gneiss consists of granulite-textured gray layers in pelitic migmatitic rocks. Composition and texture are variable, but collectively distinct from most other rock types. Chemically, the biotite-garnet gneiss is similar to calcic dacitic and primitive greywacke compositions (Wooden and Miller, 1990), but lower silica (SiO_2) versions are strongly peraluminous, suggesting a clay component, and therefore are particularly likely candidates for sedimentary rocks. Association with pelitic rocks supports a greywacke interpretation. If so, the high TiO_2 concentration of some samples indicates a cratonic or oceanic arc setting, for which mafic igneous rocks were the primary source terrane (Fig. 6).

Zircon grains from these gneisses retain characteristic crystal shapes with only minor rounding of crystal edges. Pb-Pb dates (by conventional U-Pb) of groups of grains range from 1.7 to ~2.0 Ga (Wooden and Miller, 1990). Spot analyses of single grains with the ion microprobe (SHRIMP) at Australian National University yield clusters of dates at ~2.5 Ga, ~2.3 Ga, ~1.9 Ga, and ~1.8 Ga (Fig. 7). The simplest interpretation of these dates is that they represent ages of igneous zircons from several source terranes; the older zircons were redeposited with the youngest group of syndepositional volcanic and sedimentary rocks at ~1.8 Ga.

"Paw-print" gneiss in several places appears to cut foliation in adjacent rocks, but is itself foliated. The gneiss is equigranular, felsic, and contains minor biotite. This paw-print gneiss could represent igneous dikes or possibly relatively stiff, and therefore less deformed, metasedimentary rock. Garnet pawprints in many cases are localized by boudinaged quartz-rich veins. Geochemically, the paw-print gneiss is typical of silicic to intermediate igneous rocks (65 to 71% SiO_2, 15 to 17% Al_2O_3, 5% total Fe, 2.5 to 4.5 % Ca_2O, 3 to 4.5%

Na_2O, 1.5 to 4% K_2O), roughly dacite in composition (Table 1). The similar, but garnet-rich, biotite-garnet gneiss ranges as low as 60% SiO_2 and only shows small differences in major-element chemistry from some pawprint gneiss with lower silica than most: greater TiO_2, total Fe, MnO, and MgO; and less Na_2O. Sharp differences in aluminum saturation, trace elements and rare earth elements better distinguish biotite-garnet gneiss from paw-print gneiss. Probably the higher Na_2O in paw-print gneiss results in its weakly peraluminous to slightly metaluminous composition, whereas biotite-garnet gneiss is consistently strongly peraluminous. In addition, some paw-print gneiss appears to grade into trondhjemitic compositions (M88IV-71, Table 1); these gradational rocks have lower K_2O and Rb than other paw-print gneiss. The gradation illustrates the difficulty in assigning some rocks to sedimentary and igneous protoliths, despite field appearance and chemical data.

Pelitic rocks in this lithologic group are biotite-rich, many containing minor sillimanite. In contrast to sillimanite-rich rocks at upcoming stops in lithologic group 6, we consider most of these rocks to be semi-pelites. Geochemically, pelitic and semi-pelitic rocks have 55-60% SiO_2+Al_2O_3, and are relatively high in Fe oxides, MgO and K_2O compared to other major oxides. They are extremely peraluminous (A/CNK as high as 3) and potassic. The pelites possibly represent mudstone that was interbedded with greywacke (biotite-garnet gneiss). West of the pelitic gneiss is a lithologic group typified by layers of trondhjemite.

(5) The trondhjemite lithologic group consists of pelitic gneiss, minor biotite-garnet gneiss, and distinctive light colored rocks of approximately trondhjemite composition. The light-colored rocks are granulite textured and contain quartz (25%), biotite (5-20%), and garnet (5%), the remainder being almost entirely plagioclase. Trondhjemite appears in many cases to be less deformed than neighboring gneiss, either due to younger age or different rheology. On the basis of field relations, we suspect that the trondhjemite is igneous because farther north in these mountains (Optional Stop 2), similar rock forms masses of consistent composition and igneous texture of several square kilometers in extent. The lack of interlayering with the pelitic gneiss and map relations suggest that trondhjemite intruded a pelitic sequence. Chemically (Table 1), trondhjemite also appears to be igneous: it is siliceous (69-79%), with Ca_2O and Na_2O both being more than twice as abundant as K_2O, as is typical for trondhjemite (Fig. 4), and is Mg-rich and strongly peraluminous. The trondhjemites have low Rb and total REE abundances; they generally fit a high-Al trondhjemite group. Preliminary study of zircon from trondhjemite to the north (Optional Stop 2) indicates a U-Pb-Th age of about 1755 Ma.

Calc-silicate nodules lie within several tabular trondhjemite masses that are spectacularly exposed in dry waterfalls in the upper part of the traverse. Thus far, little study of the calc-silicates has taken place. Could the calc-silicate minerals have replaced cordierite?

A few amphibolite bodies appear in the western part of the trondhjemite lithologic group, a prelude to upcoming abundant amphibolite in the pelitic lithologic group.

(6) Pelitic rocks intruded by amphibolite characterize the last lithologic group. Pelitic rocks similar to those in groups (4) and (5) are now abundant, and are interlayered primarily with amphibolite. Minor biotite-garnet gneiss is also present. Abundant sillimanite marks rocks of this group as among the most strongly pelitic in the Ivanpah Valley area. We suggest a protolith of argillite and shale for sillimanite-bearing rocks, and shaley greywacke for less pelitic rocks. Amphibolite here could represent volcanic flows and (or) intrusive rocks of basaltic composition. Elsewhere, amphibolite of tholeiitic and Mg-rich compositions clearly dikes plutonic rocks such as the meta-quartz diorite, so the amphibolites here may represent a swarm of mafic dikes. In the northern Providence Mountains, amphibolite dikes cut ~1.71 Ga granite but are metamorphosed and deformed by the ~1.7 Ga Ivanpah orogeny. All amphibolite could be essentially coeval with metamorphism and its intrusion may represent the mechanism for transferring heat to fairly shallow levels in the crust. Granitoid rocks alone are not likely to account for minimum metamorphic temperatures of 700° C (Young and others, 1989) and probable temperatures higher than the solidus temperatures of the granitoids (Thomas and others, 1988).

We will end our traverse here. If you wish to continue westward up the mountain face, you can observe a few more rock units. Pelitic gneiss grades into varied gneisses that are less pelitic and contain several types of thin bands (dikes?) of granitoid rock. A few trondhjemitic dikes are prominent; samples of these dikes have SiO_2=70% and CaO and Na_2O each 3 to 4 times as abundant as K_2O. Fairly massive granite, locally cut by abundant amphibolite and pegmatite dikes, underlies the highest point (peak 1609).

To the north (Optional Stop 2), more extensive exposures of group (5) and (6) rocks can be easily studied. Our chemical and isotopic studies in progress at the northern sites are hoped to define more closely the age and origin of trondhjemite. Retrace route to Interstate 15.

OPTIONAL TRIPS to key localities in Ivanpah Mountains

Cumulative Mileage

0.0 Begin mileage at Nipton Road/Ivanpah Road intersection. Drive south on Ivanpah Road.

1.9 Turn right on jeep track.

2.7 Straight segment of road ends. Continue on winding road in generally same direction.

3.1 Bear right at fork.

3.5 OPTIONAL STOP 1. Stop next to bold dark outcrops (Figure 2). This rock is augen gneiss containing biotite and garnet, here much less deformed than typical so that relict igneous structures are easily identified. The augen gneiss is interlayered with pelitic gneiss on the east, suggesting that some such interlayering is intrusive rather than deformational in origin. Intermixed medium-grained non-porphyritic rock also demonstrates that lithologic variations are igneous in origin. We therefore suspect that part of the heterogeneity of the more deformed granodioritic suite west of Stop 1 is also igneous in origin. This augen gneiss (M84IV-74, Table 1) is a K-rich granite, and as such represents an end-member of the intrusive rocks in the Ivanpah Mountains.

Successively toward the next big hill to the west we encounter (1) a thin sliver of metagabbro, (2) meta-quartz diorite and granodiorite, and (3) darker augen gneiss that is similar to the meta-quartz diorite body of Stop 1. The close association of dark augen gneiss with granodiorite and meta-quartz diorite, as indicated by gradational relations on both sides of the gneiss, suggests an intrusive association. Zircon studies thus far have yielded moderately discordant U-Pb results for the augen gneiss, but these data form a co-linear plot when combined with data for the meta-quartz diorite (Fig. 3). The U-Pb data for the augen gneiss are consistent with the 1.76 Ga age of the quartz diorite, but the augen gneiss could be as young as the 1710 Ma Pb-Pb ages.

The hill with lighter tones to the east is underlain mainly by pelitic gneiss and lesser biotite-garnet gneiss. Biotite-garnet gneiss sampled just below a prospect pit on the southeast face of the hill (JW86-9, Table 2) has Pb-Pb dates, for groups of zircons, of 1.8 to 2.0 Ga (Fig. 7A). Single-zircon Pb-Pb dates obtained from the SHRIMP ion probe are as old as 2.55 Ga (Fig. 7C), unequivocally demonstrating an old source terrane for these rocks. Because the biotite-garnet gneiss probably represents metamorphosed greywacke likely to be near its source terrane, that source likely was either basement for this detrital sequence or was exposed west of this (and since rifted away). Lack of deep marine basin lithologic types such as shale and chert suggests a position near continental crustal sources for greywacke, such as turbidite fan deposits.

Return to Ivanpah Road by retracing route.

OPTIONAL TRIP to lithologic groups 4, 5, and 6.

Cumulative Mileage

0.0 Begin mileage at Nipton Road/Interstate 15 interchange (overpass) but drive north (to an area not on Figure 2). Continue north through a stop sign and down a small hill to the end of pavement. Bear right (NNE) past a pump station to a dirt road marked by warning signs (for buried cable) on posts.

0.2 Small hill on left is underlain by pelitic gneiss with white leucocratic dikes and veins. Minor biotite-garnet granodiorite bands may represent dikes or volcanic flows. Amphibolite layers also cross the hill parallel to foliation. Biotite augen granodiorite gneiss underlies the east end of the hill, near the road.

1.1 Dirt track branches off to left; continue on right fork.
1.4 Left turn through gate in fence. We are going to hills straight ahead in middle distance.
3.0 Branching road to left goes to excellent outcrops of the trondhjemitic group in dry waterfalls. To see these rocks, drive to a wash 0.5 miles up the road.
3.2 Stop vehicles at foot of small hill lying in front of larger hill.

OPTIONAL STOP 2. Walk to the west, up the crest of the ridge that extends nearly to the road. The first outcrops are mainly pelitic gneiss cut by minor leucocratic veins. Foliations in these rocks dip steeply to the west; prominent lineations on garnet-quartz gneiss of probably metasedimentary origin are interspersed in the pelitic gneiss. Uphill, 1- to 10-m-thick layers of foliated amphibolite lie within the metasedimentary gneiss. Amphibolites range from hornblende-plagioclase metabasalt (sample M91IV-102, Appendix 1) to plagioclase-poor clinopyroxene-hornblende-plagioclase ultramafic rock (sample M91IV-107, Appendix 1), as they do elsewhere in the Ivanpah Valley area. These rocks can be shown to be intrusive in several places, but not in these outcrops.

Farther up hill, just above a thick mass of hornblende-plagioclase amphibolite, a rapid change in rock type takes place. The new rock is a foliated, medium-grained, light-gray biotite-garnet gneiss. Spectacular garnet is found in these light-colored gneisses where they are cut by leucocratic dikes (many of which are dismembered). Uniform composition and texture in this 10-15 m thick body suggests igneous origin as high-silica trondhjemite, but major-element chemistry (sample M91IV-101, Appendix 1) is more compatible with a sedimentary origin. Values include: SiO_2, 75.8%; Cao and Na_2O, 2.5-2.7%; and K_2O, 1.1%. Silica is much higher than, and total alkalis lower than, trondhjemites. These rocks may represent highly metamorphosed subgraywacke or immature sandstones; the ambiguities here are analogous to those for the pawprint gneiss in the Ivanpah Mountains to the south.

Upward to the crest of the first knob on this ridge, more pelitic gneiss crops out, but common thin layers of biotite gneiss and biotite-garnet gneiss indicate a less mature sedimentary component. Folds at the crest of the knob consistently are S-shaped (verge SW) and plunge gently north; these are typical of many exposed in the Ivanpah Mountains north of the I-15 freeway. Just west of the crest, starting down to the saddle, are lenses of porphyritic biotite augen gneiss. This gneiss may represent an extensively deformed margin of more homogeneous biotite-rich augen gneiss that is well exposed 50 m to the north and also in a thin band downhill to the west, nearly at the saddle. This augen gneiss, and similar rock 1 km to the west, is granodioritic in composition. Values for major-element chemistry include: SiO_2, 64-70%; CaO and Na_2O subequal, 2.5-3.5%; and K_2O, 3.0-4.5% (samples M91IV-105, M91IV-109, M91IV-110, Appendix 1). We surmise from the relatively well-preserved fabrics in the augen gneiss that the gneiss was intruded into the trondhjemite-pelitic gneiss sequence after much deformation, but prior to final deformation, related to the Ivanpah orogeny.

Amphibolite and pelitic gneiss are at the saddle. Across the saddle is a massive unit of trondhjemite gneiss that is medium- to fine-grained, highly foliated, and lithologically homogeneous. Light-gray biotite-plagioclase-quartz rock is typical; minor garnet and k-spar are present. Grain size is fairly uniform. We consider this rock, and similar rock to the west and northwest, to be intrusive. Well-developed foliation suggests a pre-Ivanpah orogeny age. Preliminary ion microprobe study of zircon from this trondhjemite indicates a U-Pb-Th age of about 1755 Ma. Values for major-element chemistry include: SiO_2 68-70%; Cao and Na_2O subequal, 3.4-4.6%; and K_2O, 1.0-2.0% (samples M91I-103, M91IV-104, M91IV-106, M91IV-108, Appendix 1).

This trondhjemite body entrains wisps of pelitic gneiss. Amphibolite (hornblende-clinopyroxene plagioclase) dikes in the trondhjemite indicate an intrusive origin for some amphibolite and further indicate a pre-Ivanpah orogeny age for the trondhjemite. Also cutting this trondhjemite body are quartz rich veins of several orientations, all foliated.

Up the ridge to the west for the next 1 km are thick groups of trondhjemitic rock and lesser amphibolite and pelitic gneiss. These rocks appear to represent a much more extensive version of groups (5) and (6)

rocks from Stop 1 in the Ivanpah Mountains. Return to vehicles and retrace route to the interchange between Nipton Road and I-15.

END OF DAY 1

DAY 2

Cumulative Mileage

0.0. Begin at I-15 exit for Nipton Road. Drive east on Nipton Road toward Searchlight (Figure 1).

1.5 The view ahead, across Ivanpah Valley, is of the New York Mountains. Capping the rounded mountains composed of Early Proterozoic rocks are the prominent dark-colored spines of the Castle Peaks, composed of Miocene andesite breccia flows. Northward are the much more rugged and higher-altitude McCullough Mountains, described by DeWitt and others (1989). West of, and below, the McCullough Mountains are the Lucy Gray Mountains. Both ranges are principally underlain by Early Proterozoic gneiss and granitoids, although a Middle Proterozoic pluton occupies much of the north end of the Lucy Gray Mountains (Anderson, 1983).

3.3 Turn right on Ivanpah Road.

6.4 Continue past the turnoff to Morningstar Mine Road (on right).

12.5 Just before (west of) the railroad crossing at the former townsite of Ivanpah, turn left on a dirt road parallel to the railroad tracks (Figure 8). Proceed parallel to the railroad, past three railroad bridges.

14.4 Turn right under the railroad bridge. A power line should cross the railroad nearby. On the east side of the railroad, avoid the extreme left and right routes–these are dry washes. Proceed east through a gate and follow the road bordered by a pipeline.

15.9 Branch left on a road diverging from the pipeline. The power line crosses overhead at this point.

16.1 Spur to the left. Continue on the right fork.

16.7 Take the left spur into the wash [those in low-clearance vehicles check the road before proceeding!] and cut sharply to the left, headed down the wash. Stop here.

16.8 STOP 1. We have stopped in Willow Wash in the northern New York Mountains (Figure 9), where much study has been focused because a long across-strike exposure of the rocks is well displayed (Elliot, 1986; Miller and others, 1986; Wooden and Miller, 1990).

Heterogeneous migmatitic layered rocks are exposed along the south wall of Willow Wash at this point. These rocks differ from those of the Ivanpah Mountains chiefly by their abundance of biotite-garnet gneiss and relative lack of pelitic rock. The rocks are typically strongly layered on scales of 1 cm to 50 cm; the main layers of light- to dark-gray biotite-garnet gneiss, amphibolite, and minor pelitic schist is further accentuated by pervasive dikes and veins of leucocratic granites. These leucocratic granites make up as much as 30% of the outcrop along Willow Wash. Abundant garnets are pervasive throughout all rocks, except amphibolites. Larger garnets, some as large as 10 cm in diameter, are sieve-textured.

Biotite-garnet gneiss is more abundant in Willow Wash than in any Proterozoic exposures we have seen in the Mojave province. Biotite-garnet gneiss here, like in the Ivanpah Mountains, contains zircon older than 1.8 Ga. As for the gneiss in the Ivanpah Mountains, we infer an immature sediment or volcanic origin. Pelitic schist, which consists of sillimanite-biotite-quartz-plagioclase, is much less common in Willow Wash than in the Ivanpah rocks of Day 1.

Amphibolite here is similar to that in the Ivanpah Mountains, consisting of three main types that overlap considerably in compositional space: High aluminum tholeiitic basalt, tholeiitic basalt, and high-magnesium ultramafic rock. We infer a similar origin, by diking during the Ivanpah orogeny, although intrusive relations are not provable at Willow Wash. Here, extrusive origins for amphibolite are permissible.

Leucocratic granites in dikes and veins carrying abundant garnet abound throughout the Willow Wash lithologic group, separating it from other, less injected, Early Proterozoic supracrustal groups in this part of the Mojave Desert. Wide dikes are composed of syenogranite and contain 74 to 76% SiO_2 and 5% K_2O (a representative sample, M84NY-68b, is given in Table 3); we have not analyzed narrower bodies that are dike-like and form pods. We believe that most leucocratic material is intrusive, probably injected from

points deeper in the crust that underwent considerable melting during the Ivanpah Orogeny. Critical observations include: 1) lack of significant amounts of melanosome argues against an *in situ* anatectic origin, 2) tabular shapes and sharp margins on many leucocratic bodies suggest intrusive origin, 3) dikes show varying development of foliation, suggesting intrusion over a span of time coincident with deformation, and (4) garnet-bearing leucocratic granite bodies cut the amphibolite, and thus are not in equilibrium with their wallrocks. In a few places, pockets of leucocratic material appear to grade into layered gneiss; these pockets may represent anatectic melt. Minor partial melting may have taken place in this part of the crust, but a significant amount of anatectic melt (leucocratic granite) migrated to this position from a deeper locus of melting. Pegmatitic textures in some leucocratic bodies suggest water-enriched melts; the hydrous melts may have been of low-viscosity and enabled migration of otherwise viscous siliceous melts. Reconciling the composition of the leucocratic granite with melting conditions and source rock is a topic in need of study.

Along exposures at the south side of the wash, a Middle Proterozoic diabase dike cuts high-grade gneisses. The diabase dike is fine grained, displays ophitic texture, and is highly altered. Nearby is another dark dike, this one of probable Miocene age. The Miocene(?) dike is aphanitic with chilled margins, and is similar to dikes that cut Cretaceous granite south of Willow Wash.

Variably developed mylonitic fabric in rocks in Willow Wash (but not near this stop) postdates the annealed fabric of granulite-facies metamorphic gneisses. Mylonitic overprints are present in bands or lenses as wide as 30 m, and affect perhaps 20% of the rock at Willow Wash. At a few locations, sillimanite is stable in the mylonites, suggesting strain while rocks were near Ivanpah orogeny metamorphic grade. However, chlorite is stable in other mylonites with similarly oriented foliations. These relations, plus the observation that ~1.1 Ga diabase dikes both cut and are cut by mylonite zones, suggest several periods of mylonitic deformation from ~1.7 Ga to after 1.1 Ga. In fact, chlorite-grade mylonite and phyllonite is typically present in zones along which Miocene volcanic rocks are displaced in ductile-to-brittle fault zones, suggesting that some chlorite may have formed during the Cenozoic. These chloritic fault zones border the McCullough Mountains and parts of the New York Mountains north of here; we will see some examples later today and drive close to many other sites of reactivated Early Proterozoic mylonitic zones.

These mylonitic rocks are more abundant eastward toward a ~1-km-wide belt of mylonite that strikes north along the west side of the crest of the New York Mountains. Similar mylonitic rocks are present in the McCullough Mountains (DeWitt and others, 1989). Westward and eastward from this belt of mylonite, the mylonitic rocks gradually decrease in abundance. The zone dips moderately westward, and lineation is fairly consistently oriented with a trend of 260 to 330°. Sense of shear is top to the east, or thrust-type movement in present orientation, in most outcrops.

Return to vehicles and proceed ~50 m down wash to where wash broadens. At this point make a very sharp right turn, up a main branch of the sandy wash along the north bank of Willow Wash. Drive past an assemblage of Proterozoic rocks similar to those just examined as we proceed up the wash.

18.4 STOP 2. Stop near a pink knob of bedrock about 2 m high within the wash near the north (left) side.

This knob and outcrops on the north side of the wash contain good exposures of the augen gneiss (Unit Xag, Figure 9) of the northern New York Mountains. The augen gneiss is a slightly sodic calc-alkaline granodiorite (Table 3). This body appears to be syn- or just pre-orogenic to the Ivanpah orogeny and has a U-Pb zircon age of 1708 ± 12 Ma (Figure 10). Margins of the augen gneiss body are tectonically interleaved with meta-supracrustal rocks and the entire augen gneiss body is foliated, indicating its pre- to syntectonic age. The augen gneiss is not as potassic as post-orogenic granitoids of the New York Mountains, and not as mafic and metaluminous as many granitoids at the Ivanpah Mountains (Table 3). Medium- to coarse-grained pink granite and pegmatite intrude the augen gneiss. This pink granite is K-rich (Table 3) and contains common allanite in dark brown spots. The pink granite was intruded generally parallel to foliation in the augen gneiss but cuts foliation at some places. The pink granite probably was emplaced late in the orogeny. Spatial coincidence of pink granite and the augen gneiss suggests they have a common origin, and thus the

augen gneiss probably is syntectonic, as are the pink granite dikes. Because the two rocks are different chemically, any relationship must be not as cogenetic intrusions but as spatially coincident intrusions from different magma sources.

We will not examine exposures farther up Willow Wash on this trip, but groups of rock different from those of the central part of the wash can be easily studied by driving up the wash to the east margin of the augen gneiss unit. Eastward from there, lithologic units containing more quartzo-feldspathic gneiss than the biotite-gneiss group we examined at stop 1 (Fig. 9) crop out. Some quartzo-feldspathic gneiss is granodioritic and tonalitic in composition, in places containing hornblende rather than garnet. Amphibolite is also common in parts of the section exposed up the wash.

Retrace the route to Ivanpah Road and return to the intersection with Nipton Road.

Cumulative mileage

0.0 Reset mileage at the Nipton Road/Ivanpah Road intersection. Proceed east on Nipton Road.

6.5 Town of Nipton, with a small store, hotel, and restaurant. No gas is available.

9.2 Border of California and Nevada.

10.7 To the south, on the right side of the highway, are low hills with prominent subhorizontal stripes. Most rock is about 1674 Ma leucocratic granite, but it is intruded by thin (1-4 m thick) sheets of biotite-rich granodiorite that create the stripes. We will examine equivalent rocks at the next stop.

12.8 Turn right on a dirt road to the south.

12.9 STOP 3. Examine outcrops along the left side of road.

Two of the four main phases of the Big Tiger plutonic complex are represented in these outcrops. The Big Tiger plutonic complex is post-orogenic, as indicated by its cross-cutting relations with foliated metamorphic rock, and crops out over a large area in the northern New York Mountains (Figures 8, 10). The main phases are (1) granodiorite of Big Tiger Wash [porphyritic], (2) granodiorite [subequigranular], (3) diorite, and (4) leucocratic granite. All phases contain biotite, and the diorite also contains hornblende. This suite of rocks contrasts in several ways with a suite of plutonic rocks farther south in the New York Mountains, the New York suite, which will be visited at Stop 5.

Variations from leucocratic granite to strongly porphyritic biotite granodiorite are present in outcrops at Stop 3; most are mylonitic gneiss at this location. Mylonitic gneiss is our term for rocks displaying folia with mylonitic textures such as grain-size reduction and ribbon quartz, but not the wholesale grain-size reduction of a mylonite. Leucocratic rock forms pods less than 2 to 100 m across in this area, which is near the center of a pluton of the porphyritic rock. Outward from the pluton, this leucocratic granite underlies many square kilometers and is indistinguishable, both in the field and analytically, from leucocratic granite forming much of the New York suite (compare the two silicic granites in Table 4--M90NY-08 is from the Big Tiger suite and M90NY-28 from the New York suite). Both granites are silicic, and contain more than 5% K_2O (Fig. 12). The porphyritic rock, informally termed the granodiorite of Big Tiger Wash, is a widespread, distinctive rock underlying most of the low hills between the crests of the New York and McCullough Mountains (sample M91NY-121, Table 4).The granodiorite of Big Tiger Wash has a U-Pb zircon age of 1672 ± 5 Ma, similar to the 1674 ± 10 Ma age for the leucocratic granite rimming it (Figure 11A, B). In this outcrop, the porphyritic granodiorite of Big Tiger Wash grades with loss of phenocrysts to coarse-grained granodiorite, which in turn grades in places to fine-grained granodiorite. Other distinctive phases of this plutonic complex are biotite-rich granodiorite, which we will see at the next stop, and diorite (samples M90NY-20, M88NY-45, Table 4).

A number of features set this Big Tiger plutonic complex apart from the other major suite of post orogeny granitoids that underlies most of the crests of the McCullough and New York Mountains. Intrusive styles differ greatly, with the Big Tiger rocks forming broadly rounded plutons, and subhorizontal intrusive sheets in places, whereas the New York suite forms subvertical intrusive sheets with common lenses and septa of supracrustal gneiss. The Big Tiger rocks are generally younger than the New York suite, although

there is some overlap in age. The Big Tiger rocks are a metaluminous calc-alkaline diorite-granodiorite-monzogranite suite (Table 4, Figure 12) that differs from not only the New York suite, but from many Early Proterozoic rocks in the Mojave province, most of which are potassium-rich peraluminous granitoids.

We suspect that the Big Tiger group of rocks, along with two smaller metaluminous plutons to the south that are ~1660 Ma (JW84-23, Table 4), represent a shift away from conditions of the Ivanpah orogeny to a crust with more typical geothermal gradient. The resulting granitoids and their intrusive styles are more typical of continental magmatic arc systems than was true earlier. In terms of age, the Big Tiger suite is part of a massive group of plutons that lies to the south and southwest across the Mojave Desert (Bender and others, 1990) and may represent the western edge of ~1.68-Ga magmatic arc rocks that sweep from the Mojave Desert across southern Colorado and northern New Mexico.

Mylonitic foliation here is moderately northwest-dipping, transitional between moderately to steeply west-dipping foliation in rocks to the south and gently west-dipping foliation in many parts of this Big Tiger plutonic complex. Map patterns for foliations suggest discrete zones of consistent orientation, some with steep dips and others with shallow dips, as if strain at the scale of tens of kilometers was controlled by conjugate shear systems. Lineation trends and plunges are fairly uniform, scattered about a trend of 266° and westward plunge of 31° (Fig. 14A), and probably indicate a uniform transport direction slightly modified by subsequent deformation. S-C fabrics, rotated porphyroblasts, and other criteria for sense of shear yield top-to-the-east shear.

13.4 Proceed south on this road, across a wash.
13.7 STOP 4. Stop on a knoll with dark bouldery outcrop.

This weathered rock is typical of coarse-grained biotite-rich granodiorite, a common phase along the southwest side of the Big Tiger plutonic complex (samples M90NY-74, M90NY-06, Table 4). Biotite in fine-grained clots is texturally similar to biotite clots in the porphyritic granodiorite of Big Tiger Wash. This connection is further supported by presence of sparse k-spar megacrysts. Additionally, the rock types are gradational over about 100 m with the change being largely the presence or absence of megacrysts. Across the wash to the northwest of this outcrop, leucocratic granite intrudes the granodiorite, as evidenced by granodiorite inclusions in the more felsic rock. Turn vehicles around at road junction 50 m ahead and return to highway 164.

14.7 Turn west on Nevada State Route 164 toward Nipton.
15.7 Turn left on the graded dirt road.
15.8 Proceed on the main route through a mine camp.
16.8 Cross the wash and stay east along the main road. Along the wash walls, Cretaceous granodiorite intrusion breccia is spectacularly exposed. We interpret this breccia as the top of a small stock. A K-Ar date of 94.4 ± 2.4 Ma (J.K. Nakata, analyst) was obtained for biotite separated from a sample collected in this wash. This area is the site of the old mining town of Crescent.
18.9 Bear right.
19.0 Bear right.
19.3 Continue straight.
20.0 Bear left at the Y junction.
20.1 Dark rocks along the road are highly altered hornblende granodiorite of Crippled Jack Well, one of a few small plutons composed of metaluminous granodiorite similar to that in the Big Tiger suite. This is the youngest rock in the Early Proterozoic suite, at 1659 Ma (Fig. 13D).
20.3 Bear left at the Y junction below the prospect.
20.5 Enter the wash and park. It is possible to drive east up the wash but the road is rough. At this stop we will walk about 1 km up fairly rough, steep hillsides.
STOP 5. We will traverse the west margin of the New York Mountains intrusive suite and look at structural zones coinciding with the margin.

Virtually all of the crest of the northern New York Mountains is underlain by plutonic rocks, most of which are leucocratic biotite monzogranite (Xlg). More biotite-rich, heterogeneous rock is present in discrete bodies that we mapped as mesocratic granite (Xmg); it is granodiorite to granite in composition. The east margin of the intrusive suite grades into wallrock in a wide zone of heavily diked migmatite, small plutons, and areas rich in garnet in the otherwise garnet-poor, biotite-bearing leucocratic granite. Screens of wallrock within the intrusive suite are subvertical and north-striking, and suggest to us that intrusion took place by repeated injection of subvertical dikes, sheets, and elongate plutons. The west margin of the intrusive suite less clearly is a gradational zone of diking because (1) it has been modified by Proterozoic mylonitization and Cenozoic faulting, and (2) it is intruded in several places by ~1.66 Ga plutons.

Begin by walking up the right branch of the wash, where thin (1 cm) to thick (60 m) mylonite zones cut leucocratic granite of the New York Mountains intrusive suite. These and other mylonite zones west of the mountain front in this area strike N10E to N30E and dip 50° to 60° west; lineations trend 305° to 028° and, taken over the area from Willow Wash to Crescent Peak, define a maximum with trend of 310° and plunge of 56° (Fig. 14B). S-C fabrics, rotated porphyroblasts, and other criteria for sense of shear yield top-to-the-east shear in more than 90% of these zones. Thus, sense of shear is the same as for mylonitic zones in the Big Tiger Wash area, but lineation orientation differs by tens of degrees. Superimposed mylonitic fabrics are not present at the intersection of these two orientation domains, suggesting that a single event produced all mylonites. The variations in orientations of mylonitic fabrics probably were caused by initial heterogeneity in flow patterns on the scale of tens of km. Granite is also cut by breccia zones, and rocks near these zones typically carry epidote and chlorite as alteration products. The breccia is Miocene because 15- to 18-Ma strata are offset (down to the west) along the zones.

Turn from the wash as it breaks into several branches and traverse steeply uphill to the south, aiming for the saddle east of a knob and in front of (west of) the steep face of the main mountain front. The knob is underlain by a thick sheet of diabase that dips steeply west; locally, it is mylonitized. The sheet is fine to medium-grained and ophitic, typical of 1.1 Ga diabase sills. At the saddle is a small fault marked by brown discolored material. At this location, stringers of amphibolite decorate the boundary between leucocratic and mesocratic granite. Boundaries between subvertical sheet-like intrusions such as these are commonly accompanied by metasedimentary rock and amphibolite of the wallrock assemblage.

Turn east and proceed uphill through exposures of leucocratic and mesocratic granite. Mesocratic granite typically contains biotite-rich granodiorite, pelitic migmatite, and amphibolite, all intermixed in swirled patterns. The assemblage is cut by garnet-bearing leucocratic dikes, another hallmark of the margins of the intrusive suite. We consider that these bodies of magma intruded as subvertical sheets, entraining screens of wallrocks that strike north. Garnet-bearing leucocratic dikes appear to record the interaction of the peraluminous magmas with the garnet-rich wall rocks. Successive intrusions along the present high ridge of the New York Mountains led to relatively massive granitoid along the axis of the intrusive suite.

Mesocratic granite is best represented in Table 4 by samples JW88-107 and B84NY-77; other samples in the lower K_2O/Na_2O group are somewhat more mafic versions of mesocratic granite. Mesocratic granite displays lower K_2O/Na_2O ratios than leucocratic granite and other, volumetrically relatively minor, high K_2O rocks (Figure 12; Table 4). In comparison with granodiorite of the Big Tiger suite, mesocratic granite is higher Al, and lower Fe, Ca, Ti, and Mg. Leucocratic granite of the New York Mountains intrusive suite is represented in Table 4 by sample B84NY-76B. In comparison with mesocratic granite, leucocratic granite is higher Si and K, and lower Ti, Fe, Ca, and Mg. In a general way, leucocratic granite is more highly evolved than mesocratic granite, which is more highly evolved than younger granodiorites of the Big Tiger suite.

The chronology of the New York Mountains intrusive suite is incompletely known at this time. Mesocratic granite yields arrays of zircon that suggest crystallization ages of about 1685 Ma (Fig. 15A). Monazite from a leucocratic granite sample yielded about 1695 Ma, which is probably close to the crystallization age of the granite. Granites in this suite near the north end of the New York Mountains and in

the McCullough Mountains both yield ages of 1685 Ma ± 12 (Fig. 15B). The pattern of ages suggests that the intrusive suite consists of granitoids intruded over the period 1695 to 1685, but details of times of intrusion for individual bodies and the upper and lower bounds for the group of plutons are not precisely known.

As at Willow Wash and Big Tiger Wash, mylonitic rocks along the west side of the New York Mountains form a ~1-km wide zone that grades into less deformed rocks to the east and west by decreasing numbers of individual, narrow mylonite zones. All rocks display structures with similar geometric elements, suggesting that the zone formed during a single kinematic regime. However, conflicting evidence for the age of mylonitic rocks suggests that different parts of the zone were active from times as early as 1.66 Ga and as late as 1.1 Ga. For instance, sillimanite+muscovite is stable in parts of the zone in Willow Wash, suggesting metamorphic conditions during mylonitization that were similar to those during the Ivanpah orogeny. A 1.66-Ga granodiorite pluton near that site is highly elongate within a narrow mylonite zone that is essentially restricted to outcrop of the granodiorite, suggesting deformation while the body was hot and localization of strain at the site of intrusion. In contrast, 1.1 Ga diabase dikes both cut and are cut by mylonitic zones. Zones that cut the dikes contain stable chlorite, rather than micas that are stable in zones cut by the diabase, and generally lineation is not well preserved in these later, lower-temperature zones. The mylonite zone apparently underwent reactivation at one or more times following initial formation at 1.66 Ga or earlier. The timing of mylonitization following the Ivanpah orogeny and during gradual(?) cooling of the rocks is at first glance difficult to reconcile with the present thrust geometry of the zone (top up to the east). Tectonic unroofing (normal faulting) seems to be a more likely scenario. However, similarly oriented mylonitic zones of about the same age are present in western Arizona (Karlstrom and Bowring, 1988) and in several other places in the eastern Mojave Desert. Thrusting may have taken place within and near the margin of the magmatic arc represented by the voluminous post-orogenic granitoids of the region. Such thrusting is described near the margins of Mesozoic magmatic arcs (e.g., Walker and others, 1990a,b; Dunne and others, 1978, 1983).

Return to the vehicles, and retrace the roads to Nevada State Route 164 (Nipton Road).

END OF DAY 2

DAY 3

Cumulative Mileage

0.0 Begin at intersection of Walking Box Ranch Road and Nevada State Route 164, 7.0 miles west of Searchlight, Nevada (Figure 1). Proceed south on Walking Box Road. Stay on the oiled road through the ranch. The view ahead is of Castle Peaks. To the left at 10:00 are the Castle Mountains (Miocene volcanic rocks) and on the right are the New York Mountains (Early Proterozoic rocks).

7.6 Corral. Turn right (west) through the gate, then turn south and out of the corral. Road follows a fence.

8.9 Follow the road through the corral and turn right, up the wash, at the corral exit.

9.8 STOP 1. Stop at a large outcropping of white and pink, coarse-grained granitic rock cutting highly folded biotite-rich migmatite and minor amphibolite.

The migmatite contains thin layers of biotite-garnet gneiss. This assemblage is typical of gneisses east of the New York Mountains intrusive suite (Figure 11), with the swirled biotite-rich migmatite being most distinctive. The pegmatite probably is related to the New York suite because it is found within the east margin of these intrusive rocks and is interlayered with adjacent gneisses.

Return to vehicle and continue up wash to less weathered outcrops.

10.0 STOP 2. A short distance up the wash, complexly folded biotite migmatite is cut by a small linear body of mesocratic granite (Xmg), a distinctive rock of the New York suite.

The mesocratic rock is prominently garnet-spotted, biotite monzogranite that is subequigranular, medium to coarse grained, and ubiquitously inhomogeneous, characterized by swirled patterns of biotite or

quartz-rich rock. The granite is unfoliated, so is younger than metamorphic rocks of the Ivanpah Orogeny such as the migmatite it cuts. Garnet here is an indicator that the rocks are located along the margin of the intrusive suite; mesocratic granite within the interior of the suite does not carry garnet.

White and pink pegmatite dikes cut the mesocratic granite along this eastern wall zone of the intrusive suite. Also in this zone of interfingering wallrock and intrusive rock are abundant large garnets, a feature not seen in the center of the intrusive suite. Bodies of mesocratic and leucocratic granite, that together comprise the New York Mountains intrusive suite, are elongate north-south and dip nearly vertically. The bodies typically are bounded by screens and panels of diked migmatite, suggesting to us a sheeted emplacement form.

Walk up the wash to examine the interfingering styles of plutonic units and wallrocks. About 0.8 km up the wash, bold outcrops on the south side expose a pre-tectonic intrusive rock. The rock is homogeneous biotite granodiorite gneiss that is modestly porphyritic with K-spar augen as large as 1.5 cm. It is well-foliated and diked by more leucocratic rock. This gneiss is about 1.73 Ga on the basis of Pb studies of zircon, and is chemically distinct from post-Ivanpah orogeny magmas.

If one continues, on foot or by car, up the wash another 1 to 2 km, the main intrusive suite is encountered and garnet-bearing granitoids gradually lessen in abundance. We interpret the loss of garnet as indicating less interaction with incorporated wallrock.

Return to the vehicles and drive down the wash to the road at the corral.

11.1 Turn left on the road through the corral.

12.5 Turn right on the oiled road, headed south. We pass through the Castle Mountains. Miocene volcanic rocks were described by Turner and Glazner (1990).

21.4 Turn right on the graded gravel road (west). The high southern New York Mountains, visible at 10 o'clock, are underlain by Cretaceous granite.

22.3 Oblique intersection. Continue west.

24.0 Ignore road branching off to right.

24.5 Intersection with road along old railroad grade. Bear left (south). A good exposure of mesocratic and leucocratic granite of the New York Mountains intrusive suite can be seen by detouring from this point. To see this extra outcrop, turn north on the railroad grade road for 0.9 miles, then turn west on a jeep road. In about 2.1 miles, pass an earth dam on a rough stretch of volcanic rocks, and bear due north on the road for about 1.2 miles. At this point, the hill on the right and outcrops adjacent to the road are underlain by the two main granitoids (leucocratic and mesocratic granite) of the New York Mountains, which are cut by ~1.1 Ga diabase here.

29.2 Townsite of Barnwell (Figure 8). Turn left on the road toward Lanfair. Wind through ridges of Tertiary gravel and sparse exposures of Miocene volcanic rocks.

36.4 Ox Ranch. Continue south.

41.6 Lanfair. Turn right on the graded road.

44.2 Sharp curves to avoid a hill of Paleozoic carbonate rock.

47.5 Sharp right turn.

48.5 Sharp left turn.

50.6 Enter Watson Wash.

51.0 Short road on the left leads to Rock Spring, a Native American site and type locality of the mid-Cretaceous Rock Spring Monzodiorite of Beckerman and others (1982). Although the Rock Spring Monzodiorite originally was considered Jurassic(?) by Beckerman and others (1982), zircon from it was dated at ~98 Ma by Ed DeWitt (1985, oral commun). To the east of Rock Spring, the road parallels the south flank of Pinto Mountain, a horizontally-striped mountain with spectacular exposures of the several outflow units of the Miocene Wild Horse Mesa Tuff (McCurry, 1988).

58.4 Turn left on Black Canyon Road.

61.2 Turn right to Mid Hills campground (Wild Horse Canyon Road). The Mid Hills Adamellite of Beckerman and others (1982) is exposed just before this intersection, where a well and corral lie next to the road. The granite is about 93 Ma (Miller and others, 1994).

63.1 Continue straight past the Mid Hills campground turnoff.

66.7 Turn right on a jeep road (Macedonia Canyon Road), and through the gate. Caution: this road traverses very soft sand in several places.

67.9 STOP 3. Gneiss of Macedonia Canyon (Figure 1).

Exposed along the south wall of Macedonia Canyon is prominently striped, felsic gneiss informally named for these exposures and several black amphibolite dikes. The gneiss is peraluminous, coarse- to medium-grained, biotite monzogranite with stripes defined by thin zones of more abundant garnet and biotite; it contains dismembered layers of amphibolite. Leucocratic segregations or veins in the gneiss are deformed in the highly folded complex. Blebs of biotite, about 0.5 to 1.0 cm diameter, are a conspicuous feature of the gneiss. Minor relic garnet is preserved in some of these blebs. Textural similarity with garnet-rich granite gneisses in the New York Mountains suggests to us that this rock once was garnet-biotite granite gneiss of igneous origin. We suspect that most garnet was retrograded when the nearby Late Cretaceous Mid Hills Adamellite was emplaced. The roof of the Mid Hills pluton is exposed in several places along canyon walls of the west side of the Providence Mountains, where it is a gently south-dipping surface (Goldfarb and others, 1988; Miller and others, 1991). We consider the highly deformed to migmatitic character of the gneiss of Macedonia Canyon to indicate an origin as a pre-orogenic to synorogenic igneous complex.

Amphibolite bodies at Macedonia Canyon are deformed similarly to the enclosing gneiss. Chemically, they are alkalic tholeiites. We have not identified high-Mg ultramafic amphibolites, comprising part of the amphibolite suite in the Ivanpah and New York Mountains, in this area.

The gneiss of Macedonia Canyon crops out over a 10 x 15 km area (Goldfarb and others, 1988), but shows only minor chemical, petrologic, and textural variation. The uniform granitic composition implies igneous origin (Table 5). Two possibilities are (1) a thick pile of rhyolite with a few basalt flows, or (2) a large plutonic complex cut by basalt dikes. We feel that locally crosscutting, distinctive textural phases reminiscent of porphyritic textures and otherwise remarkably uniform composition for the gneiss of Macedonia Canyon point strongly to a plutonic origin. Emplacement of the plutonic complex probably was accomplished with much entraining of wallrock screens. Similar metaplutonic rocks crop out to the west in the Kelso Mountains and nearby parts of Cima Dome (Fig. 1), making this mass of gneiss one of the largest pre/syn-Ivanpah orogeny masses of granite known in the Mojave Desert.

Zircon studied in three samples yielded similar data indicating a U-Pb age of about 1.71 Ga for the gneiss of Macedonia Canyon (Fig. 16), which is compatible with an early- to syn-orogenic origin. Thus, voluminous plutonism and mafic diking were part of the Ivanpah orogeny in the Providence Mountains. Considerable deformation took place during and (or) after intrusion.

END OF TRIP

Return to Wild Horse Canyon Road and go south to Black Canyon Road, to eventually reach I-40 and routes east to Needles and points in Arizona. Continue down Macedonia Canyon Road to Morningstar Mine Road for routes to Amboy and Baker, California, and Las Vegas, Nevada.

REFERENCES CITED

Anderson, J.L., 1983, Proterozoic anorogenic granitic plutonism of North America, *in* Medaris, L.G., ed., Proterozoic geology; Selected papers from an international Proterozoic symposium: Geological Society of America Memoir 161, p. 133-154.

Beckerman, G.M., Robinson, J.P., and Anderson, J.L., 1982, The Teutonia batholith: A large intrusive complex of Jurassic and Cretaceous age in the eastern Mojave Desert, California, *in* Frost, E.G., and Martin, D.L., eds., Mesozoic-Cenozoic tectonic evolution of the Colorado River region, California, Arizona, and Nevada: San Diego, Cordilleran Publishers, p. 205-220.

Bender, E.E., Miller, C.F., and Wooden, J.L., 1990, The Fenner Gneiss and associated units: An Early Proterozoic composite batholith, Piute and Old Woman Mountains, Calif. [abs.]: Geological Society of America Abstracts with Programs, v. 22, p. 7.

Bennett, V.C., and DePaolo, D.J., 1987, Proterozoic crustal history of the western United States as determined by neodymium isotopic mapping: Geological Society of America Bulletin, v. 99, p. 674-685.

Bhatia, M.R., 1983, Plate tectonics and geochemical compositions of sandstone: Journal of Geology, v. 21, p. 611-627.

Burchfiel, B.C., and Davis, G.A., 1977, Geology of the Sagamore Canyon-Slaughterhouse Spring area, New York Mountains, California: Geological Society of America Bulletin, v. 88, p. 1623-1640.

DeWitt, Ed, Anderson, J.L., Barton, H.N., Jachens, R.C., Podwysocki, M.H., Brickey, D.W., and Close, T.J., 1989, Mineral resources of the South McCullough Mountains Wilderness Study Area, Clark County, Nevada: U.S. Geological Survey Bulletin 1730, 24 p.

DeWitt, Ed, Armstrong, R.L., Sutter, J.F., and Zartman, R.E., 1984, U-Th-Pb, Rb-Sr, and Ar-Ar mineral and whole-rock isotope systematics in a metamorphosed granitic terrane, southeastern California: Geological Society of America Bulletin, v. 95, p. 723-739.

DeWitt, Ed, Kwak, L.M., and Zartman, R.E., 1987, U-Th-Pb and 40Ar/39Ar dating of the Mountain Pass carbonatite and alkalic igneous rocks, southeastern California [abs.]: Geological Society of America Abstracts with Programs, v. 19, p. 642.

Dunne, G.C., Gulliver, R.M., and Sylvester, A.G., 1978, Mesozoic evolution of the White, Inyo, Argus, and Slate Ranges, eastern California, *in* J.H. Stewart, C.H. Stevens, and A.E. Fritsche, eds., Paleozoic Paleogeography of the Western United States: Pacific Section, Society of Economic Paleontologists and Mineralogists, Paleogeography Symposium 2, p. 189-207.

Dunne, G.C., Moore, S.C., Gulliver, R.M., and Fowler, J., 1983, East Sierran thrust system, eastern California [abs.]: Geological Society of America Abstracts with Programs, v. 15, p. 322.

Elliot, G.S., 1986, Early Proterozoic high-grade metamorphic rocks of Willow Wash, New York Mountains, southeastern California: San Jose, CA, San Jose State University, M.S. thesis, 110 p.

Foster, D.A., Miller, C.F., Harrison, T.M. and Hoisch, T.D., 1992, 40Ar/ 39Ar thermochronology and thermobarometry of metamorphism, plutonism, and tectonic denudation in the Old Woman Mountains area, California: Geological Society of America Bulletin, v. 104, p. 176-91.

Goldfarb, R.J., Miller, D.M., Simpson, R.W., Hoover, D.B., Moyle, P.R., Olson, J.E., and Gaps, R.S., 1988, Mineral resources of the Providence Mountains Wilderness Study Area, San Bernardino County, California: U.S. Geological Survey Bulletin 1712-D, 70 p.

Hewett, D.F., 1956, Geology and mineral resources of the Ivanpah Quadrangle, California and Nevada: U.S. Geological Survey Professional Paper 275, 172 p.

Karlstrom, K.E., and Bowring, S.A., 1988, Early Proterozoic assembly of tectonostratigraphic terranes in southwestern North America: Journal of Geology, v. 96, p. 561-76.

McCurry, M.O., 1988, Geology and petrology of the Woods Mountains volcanic center, southeastern California: Implications for the genesis of peralkaline rhyolite ash flow tuffs: Journal of Geophysical Research, v. 93, no B12, p. 14,835-14,855.

Miller, D.M., and Wooden, J.L., 1993, Geologic map of the New York Mountains area, California and Nevada: U.S. Geological Survey Open-File Report 93-98, 19 p.

Miller, D.M., Frisken, J.G., Jachens, R.C., and Gese, D.D., 1986, Mineral resources of the Castle Peaks Wilderness Study Area, San Bernardino County, California: U.S. Geological Survey Bulletin 1713-A, 17 p.

Miller, D.M., Walker, J.D., De Witt, Ed, and Nakata, J.K., 1994, Mesozoic episodes of horizontal crustal extension, U.S. Cordillera [abs.]:Geological Society of America Abstracts with Programs, v. 26, no. 2, p. 74.

Miller, D.M., Miller, R.J., Nielson, J.E., Wilshire, H.G., Howard, K.A., and Stone, Paul, compilers, 1991, Preliminary geologic map of the East Mojave National Scenic Area, California: U.S. Geological Survey Open-File Report 91-435, 8 p., scale 1:100,000.

Nielson, J.E., Lux, D.R., Dalrymple, G.B., and Glazner, A.F., 1990, Age of the Peach Springs Tuff, southeastern California and western Arizona: Journal of Geophysical Research, v. 95, p. 571-580.

Spencer, J.E., and Reynolds, S.J., 1991, Tectonics of mid-Tertiary extension along a transect through west central Arizona: Tectonics, v. 10, p. 1204-1221.

Thomas, W.M., Clarke, H.S., Young, E.D., Orrell, S.E., and Anderson, J.L., 1988, Proterozoic high-grade metamorphism in the Colorado River region, Nevada, Arizona, and California, *in* Ernst, W.G., ed., Metamorphism and crustal evolution of the western United States, Rubey Volume VII: Englewood Cliffs, Prentice Hall, p. 526-537.

Turner, R.D., and Glazner, A.F., 1990, Miocene volcanism, folding and faulting in the Castle Mountains, southern Nevada and eastern California, *in* Wernicke, B.P., ed., Cenozoic tectonics of the Basin and Range Province at the latitude of Las Vegas: Geological Society of America Memoir 176, p. 23-25.

Walker, J.D., Martin, M.W., Bartley, J.M., and Coleman, D.S., 1990a, Timing and kinematics of deformation in the Cronese Hills, California, and implications for Mesozoic structure of the southwestern Cordillera: Geology, v. 18, p. 554-557.

Walker, J.D., Martin, M.W., Bartley, J.M., and Glazner, A.F., 1990b, Middle to Late Jurassic deformation belt through the Mojave Desert, California [abs.]: Geological Society of America Abstracts with Programs, v. 22, no. 3, p. 91.

Wooden, J.L., and DeWitt, E., 1991, Pb isotopic evidence for the boundary between the Early Proterozoic Mohave and Central Arizona crustal provinces in western Arizona, *in* Karlstrom, K.E., ed., Proterozoic Geology and Ore Deposits of Arizona: Arizona Geological Society Digest 19, p. 27-50.

Wooden, J.L., and Miller, D.M., 1990, Chronologic and isotopic framework for Early Proterozoic crustal evolution in the eastern Mojave Desert region, southeastern California: Journal of Geophysical Research, v. 95, no. B12, p. 20,133-20,146.

Wooden, J.L., Stacey, J.S., Howard, K.A., Doe, B.R., and Miller, D.M., 1988, Pb isotopic evidence for the formation of Proterozoic crust in the southwestern United States, *in* Ernst, W.G., ed., Metamorphism and crustal evolution of the western United States, Rubey Volume VII: Englewood Cliffs, Prentice Hall, p. 69-86.

Young, E.D., 1989, Petrology of biotite-cordierite-garnet gneiss of the McCullough Range Nevada II. *P-T-aH_2O* path and growth of cordierite during late stages of low granulite-grade metamorphism: Journal of Petrology, v. 30, pt. 1, p. 61-78.

Young, E.D., Anderson, J.L., Clarke, H.S., and Thomas, W.M., 1989, Petrology of biotite cordierite-garnet gneiss of the McCullough Range, Nevada I. Evidence for Proterozoic low-pressure fluid-absent granulite-grade metamorphism in the southern Cordillera: Journal of Petrology, v. 30, pt. 1, p. 39-60.

Young, R.A., and Brennan, W.J., 1974, Peach Springs Tuff: Its bearing on structural evolution and development of Cenozoic drainage in Mohave County, Arizona: Geological Society of America Bulletin, v. 85, p. 83-90.

FIGURE CAPTIONS

Figure 1. Geography of the northeastern Mojave Desert and locations of field trip stops. Exposures of Proterozoic rocks are shaded.

Figure 2. Geologic map of Proterozoic rocks, east part of Ivanpah Mountains, and correlation of map units. See description of DAY 1, STOP 1 for full description of map units. Map base is Mineral Hill, California, 7.5-minute quadrangle. Contour interval is 10 m. From unpublished mapping of D.M. Miller and J.L. Wooden.

Figure 3. U-Pb concordia diagram for the meta-quartz diorite, leucocratic phase of the meta-quartz diorite, and augen gneiss, Ivanpah Mountains. All data for samples are essentially co-linear; regression line shown is for all samples.

Figure 4. Plots of major-element chemistry for metaigneous rocks in the Ivanpah Mountains, keyed to types described for Day 1, Stop 1 (more data are plotted than are given in tables). A. Na_2O and K_2O vs. SiO_2. Low K_2O and high SiO_2 for trondhjemite sets it apart from the higher K_2O, slightly lower-SiO_2 granitoids. Sodic field includes meta-quartz diorite gneiss and hornblende-bearing granodioritic gneiss from the southern Ivanpah Mountains. Biotite-rich granodiorite gneiss is not plotted for clarity; these rocks display K_2O about equal to Na_2O and therefore lie between the suites shown. B. Na_2O vs. total Fe calculated as Fe_2O_3. Hornblende-bearing sodic granodiorite lies closer to trondhjemite field than do other granitoids.

Figure 5. Plots of major-element chemistry for amphibolite and gabbro, Ivanpah and New York Mountains (more data are plotted than are given in tables). A. Al_2O_3 vs. MgO. Tholeiitic basalt chemistry can be subdivided by distinguishing a high-Al type. High-Mg amphibolite forms a distinct group. Gabbro is similar to high-Al tholeiites. B. Total Fe (calculated as FeO)/MgO vs. Al_2O_3. Variation in Fe does not change the three main groupings of amphibolites, although it adds scatter.

Figure 6. TiO_2 discrimination diagram for graywacke (more data are plotted than are given in tables). The lower silica, aluminum- and iron-rich examples of biotite-garnet gneiss, which are the most suitable rocks for graywacke protolith, plot as oceanic-arc graywackes. Plot after Bhatia (1983).

Figure 7. U-Pb plots for zircon samples from biotite-garnet gneiss. A. Conventional concordia diagram for samples from the Ivanpah Valley region. Symbols identify locations, but several different samples are combined for each location. Pb-Pb dates for groups of zircons are 1.7 to 1.9 Ga. B. Cumulative frequency plot of Pb-Pb dates for conventional analyses, showing steps that may indicate discrete sources. C. Cumulative frequency plot of Pb-Pb dates for single-zircon analyses, showing steps similar to those from conventional data, but also showing Archean source.

Figure 8. Simplified geologic map of northern New York Mountains, modified from Miller and Wooden (1993). Locations for trip stops on DAY 2 and DAY 3 are shown (2-1 indicates day 2, stop 1, etc.). Locations of Figures 9 and 11 are outlined.

Figure 9. Geologic map reproduced from Miller and Wooden (1993), showing rock units and structure in area of Willow Wash. See Figure 8 for location. Locations of DAY 2 STOPS 1 and 2 are shown with conventions of Figure 8.

Figure 10. U-Pb concordia diagram for augen gneiss in Willow Wash, New York Mountains.

Figure 11. Geologic map reproduced from Miller and Wooden (1993), showing rock units and structure in northern New York Mountains. See Figure 8 for location. Locations of DAY 2 STOPS 3 to 5, and DAY 3 STOPS 1 and 2 are shown with conventions of Figure 8. Map units, correlation, symbols, and scale given in Figure 9.

Figure 12. Plots of geochemical data for New York Mountains granitoids (more data are plotted than are given in tables). Leucocratic granite (Xlg) is represented as high-silica granite, and mesocratic granite (Xmg) is represented as the low K_2O/Na_2O group. The Big Tiger intrusive suite (except the leucocratic granite) and granodiorite of Crippled Jack Well are labelled "metaluminous"; samples that correspond to specific rocks

units are identified in the text. A. SiO_2 vs. aluminum saturation ($Al_2O_3/CaO + Na_2O + K_2O$ on molecular basis) shows that many granitoids are moderately peraluminous. Peraluminous rocks group less tightly on other plots. B. K_2O/Na_2O vs. SiO_2 plot shows a spread in alkalis in the peraluminous rocks.

Figure 13. U-Pb concordia diagram for granitoids of the Big Tiger plutonic complex and related metaluminous rocks. A. Granodiorite of Big Tiger Wash. B. Leucocratic granite spatially associated with the Big Tiger plutonic complex. C. Dike rock similar to granodiorite of Crippled Jack Well, but in the margin of the Big Tiger plutonic complex. D. Pluton considered part of the granodiorite of Crippled Jack Well, exposed near Moore railroad siding.

Figure 14. Lower hemisphere, equal-area plots of mylonitic lineations in the New York and McCullough Mountains. Contoured by Kamb method, 3-sigma significance level, using Macintosh software developed by R.W. Allmendinger.

Figure 15. U-Pb concordia diagram for granitoids of the New York Mountains intrusive suite. A. Granodiorite and granite assigned to the mesocratic granite (Xmg) map unit. Individual samples yield upper-intercept ages close to that determined by the composite group, but individual errors are large. Composite error accounts for scatter of individuals. Slightly biotite-enriched leucocratic granite sampled at north tip of New York Mountains.

Figure 16. U-Pb plot for gneiss of Macedonia Canyon. Sample M83MH-92 yields a 1710 ± 9 Ma upper intercept. Other samples are co-linear and probably the same age, but do not define chords that are as precise.

TABLE CAPTIONS

Table 1. Representative analyses of metaigneous gneisses – Ivanpah Mountains.

Table 2. Representative analyses of metasedimentary rocks and amphibolites– Ivanpah Mountains.

Table 3a. Representative analyses of metaigneous rocks – Willow Wash and vicinity, New York Mountains.

Table 3b. Representative analyses of metasupracrustal rocks – Willow Wash and vicinity, New York Mountains.

Table 3c. Representative trace element analyses of rocks – Willow Wash and vicinity, New York Mountains.

Table 4. Representative analyses of post-Ivanpah Orogeny granitoids.

Table 5. Representative analyses of metaigneous rocks – North Providence Mountains.

APPENDIX CAPTIONS

Appendix 1. Chemistry data for Proterozoic rocks, Optional Stop 2, Day 1.

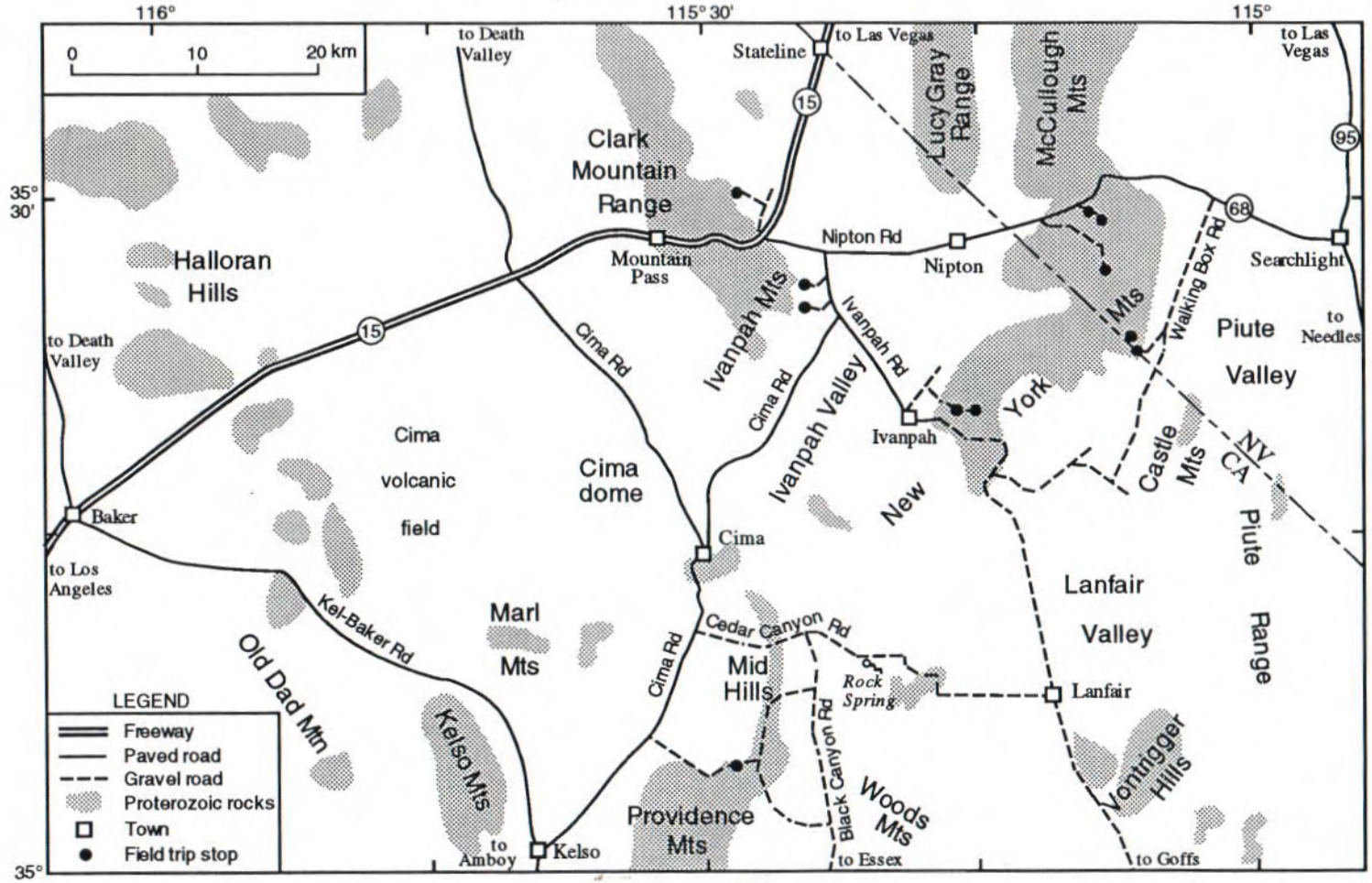
116°
115° 30'
115°
0
10
20 km
to Death Valley
Stateline
to Las Vegas
to Las Vegas
Lucy Gray Range
McCullough Mts
Clark Mountain Range
35° 30'
Halloran Hills
Mountain Pass
Nipton Rd
Nipton
Searchlight
to Needles
Walking Box Rd
Piute Valley
Ivanpah Mts
Ivanpah Rd
Cima Rd
Ivanpah Valley
Ivanpah
York
Castle Mts
NV
CA
Piute Range
Cima volcanic field
Cima dome
New
Baker
to Los Angeles
Cima
Lanfair Valley
Kel-Baker Rd
Marl Mts
Old Dad Mtn
Cedar Canyon Rd
Mid Hills
Rock Spring
Lanfair
Kelso Mts
Black Canyon Rd
Woods Mts
Ventnigger Hills
to Amboy
Kelso
Providence Mts
to Essex
to Goffs
35°
LEGEND
Freeway
Paved road
Gravel road
Proterozoic rocks
Town
Field trip stop

Figure 1.

LEGEND

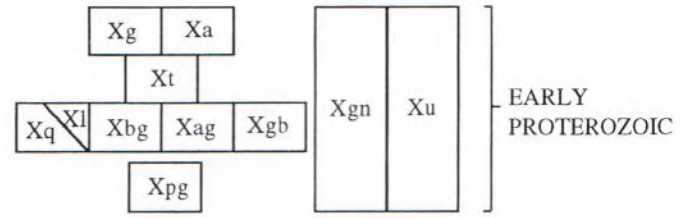

CONTACT--Dotted where covered

65 HIGH-ANGLE FAULT--Dashed where location inferred, dotted where concealed; dip indicated; bar and ball on downthrown side

18 ORIENTATION OF FOLIATION

Xg	Granite
Xa	Amphibolite
Xt	Trondjhemite
Xq	Quartz diorite
Xl	Leucocratic rocks
Xbg	Biotite-rich granodiorite
Xag	Augen gneiss
Xgb	Gabbro
Xpg	Pelitic gneiss
Xgn	Gneissic rocks
Xu	Undivided gneissic rocks

Figure 2. Legend.

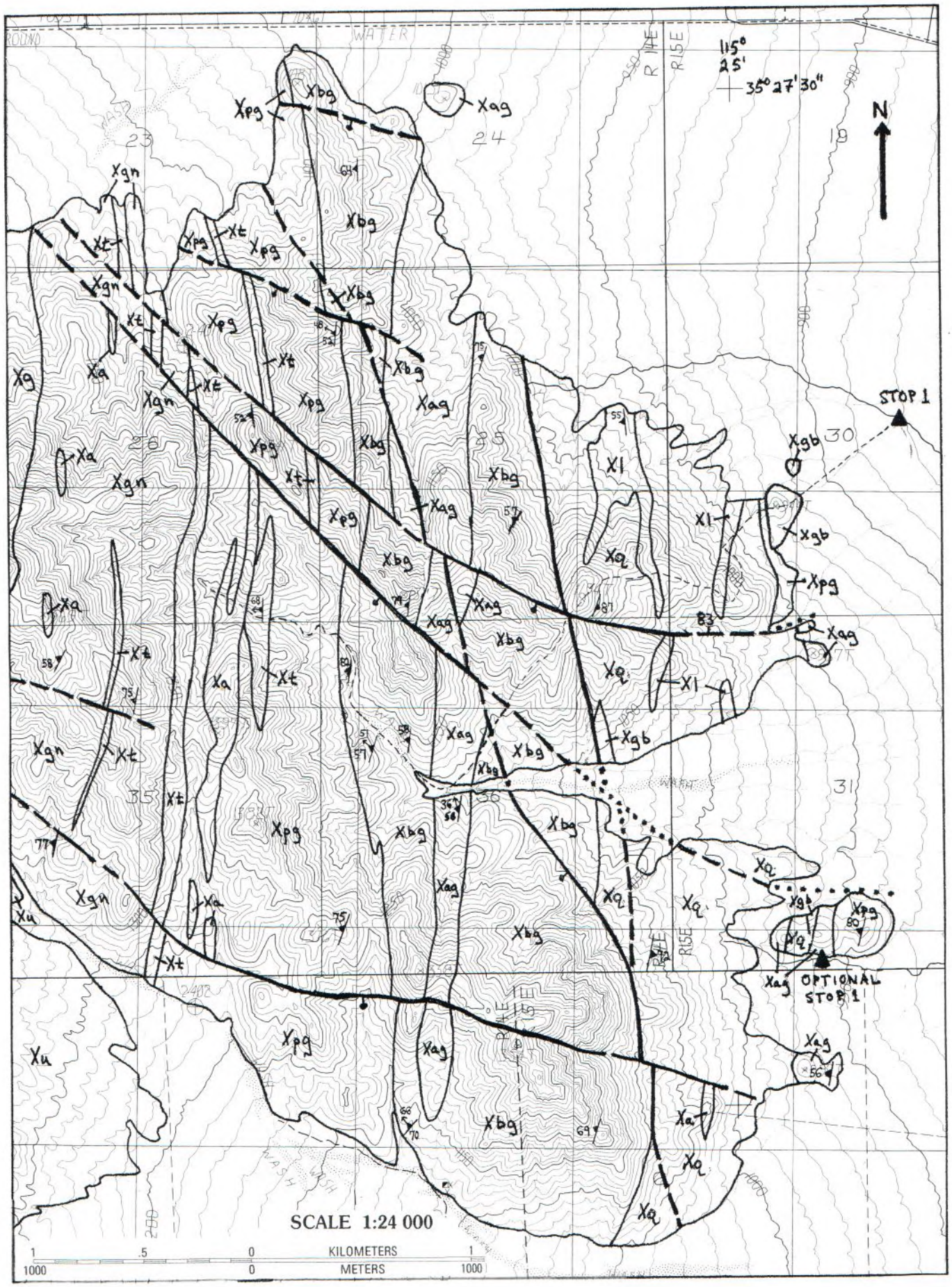
115° 25'
35° 27' 30"
N
STOP 1
OPTIONAL STOP 1
SCALE 1:24 000
KILOMETERS
METERS

Figure 2.

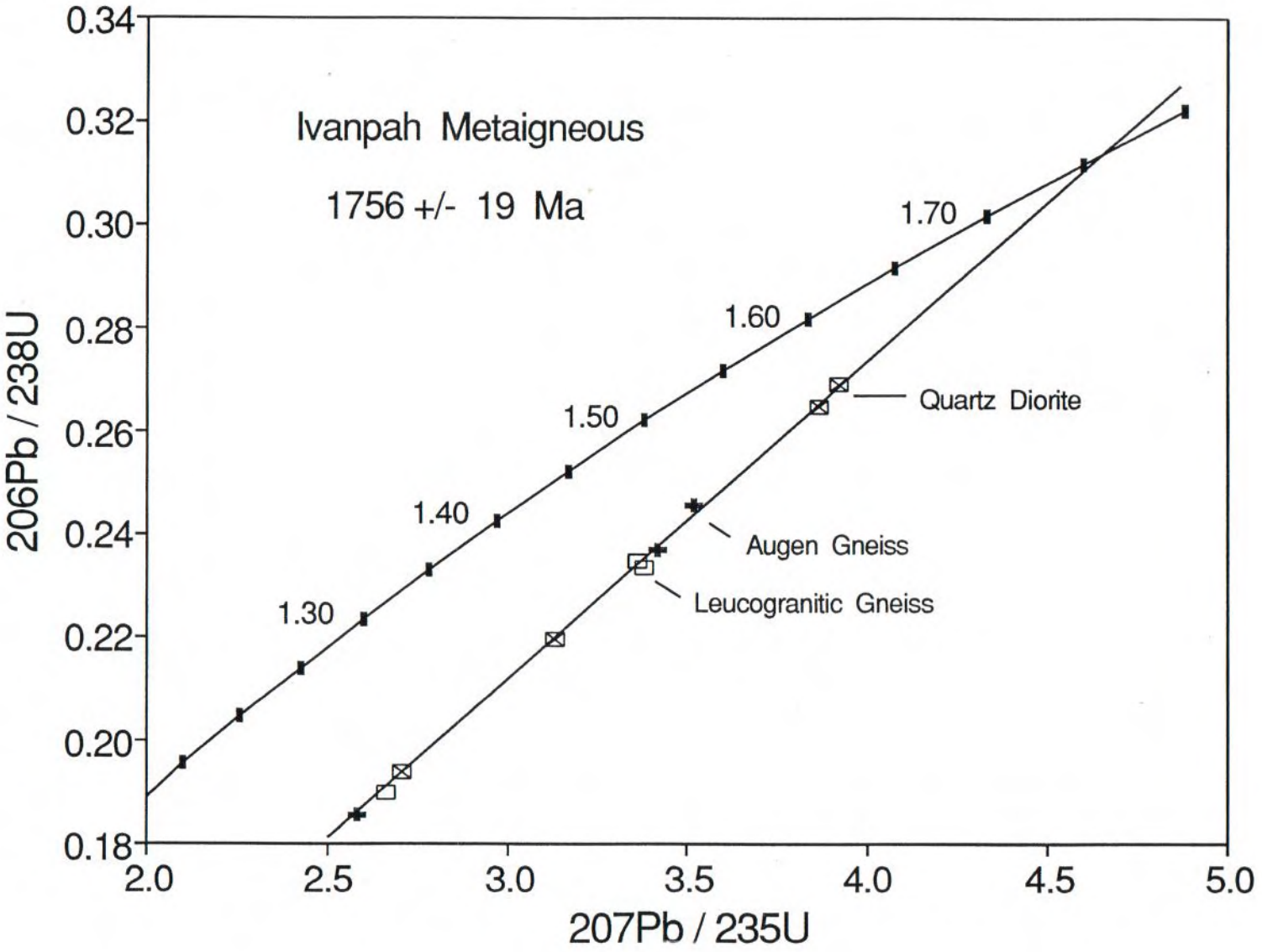
Ivanpah Metaigneous
1756 +/- 19 Ma
1.70
1.60
1.50
1.40
1.30
Quartz Diorite
Augen Gneiss
Leucogranitic Gneiss
206Pb / 238U
207Pb / 235U
0.34
0.32
0.30
0.28
0.26
0.24
0.22
0.20
0.18
2.0
2.5
3.0
3.5
4.0
4.5
5.0

Figure 3.

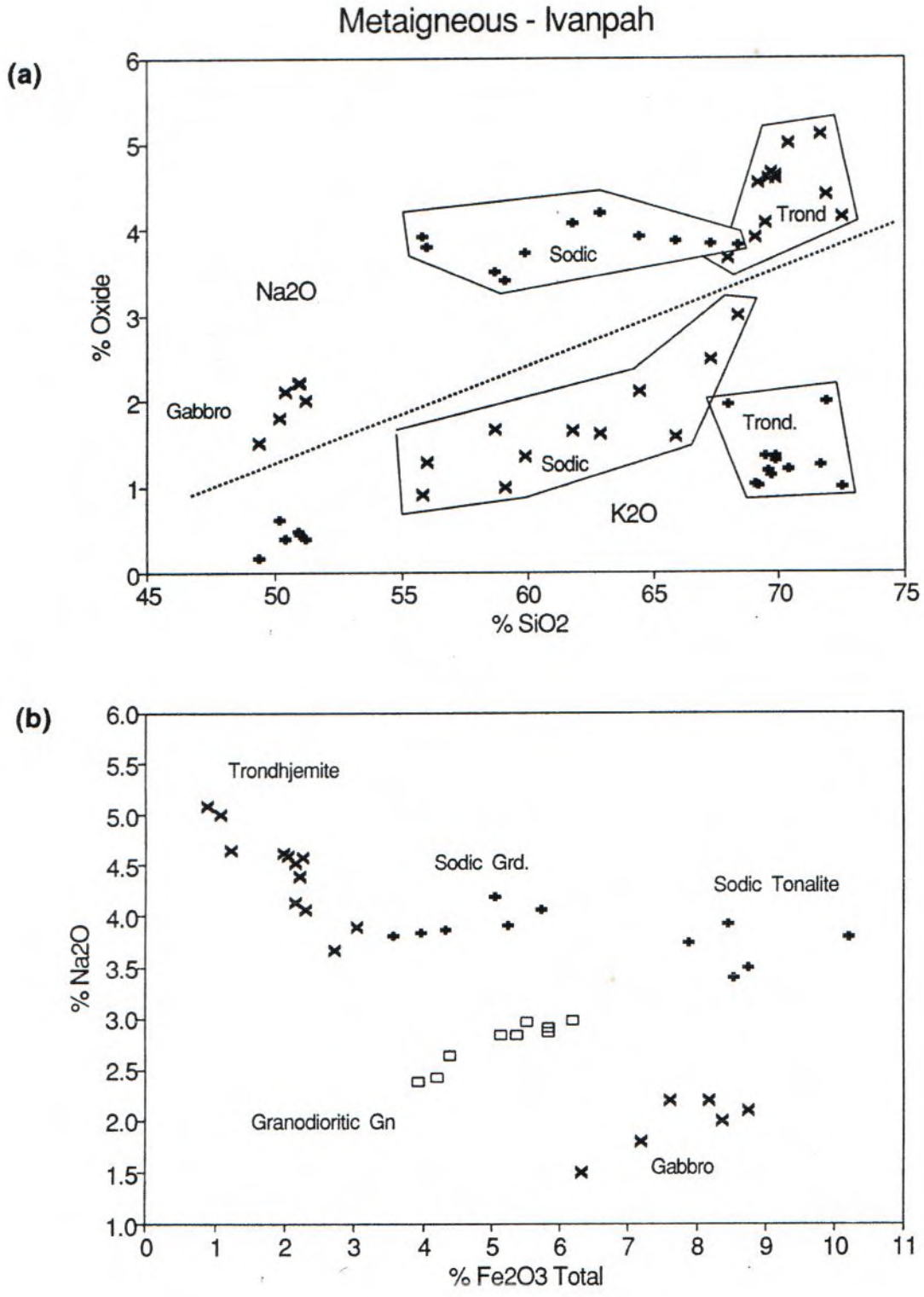
Metaigneous - Ivanpah
(a)
% Oxide
% SiO2
Na2O
K2O
Gabbro
Sodic
Trond
Sodic
Trond.
(b)
% Na2O
% Fe2O3 Total
Trondhjemite
Sodic Grd.
Sodic Tonalite
Granodioritic Gn
Gabbro

Figure 4.

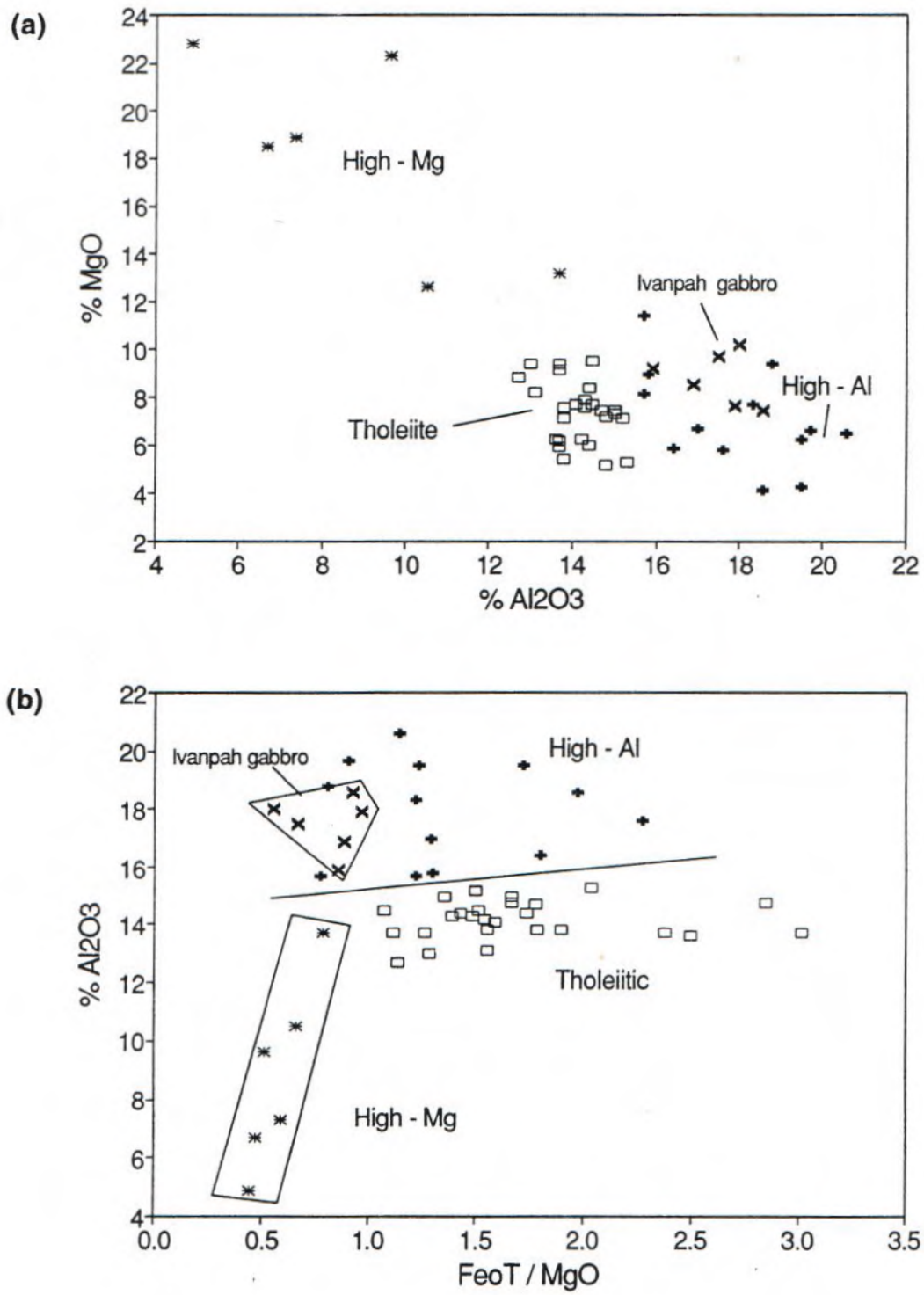
(a)
% MgO
% Al2O3
High - Mg
Ivanpah gabbro
High - Al
Tholeiite
(b)
% Al2O3
FeoT / MgO
Ivanpah gabbro
High - Al
Tholeiitic
High - Mg

Figure 5.

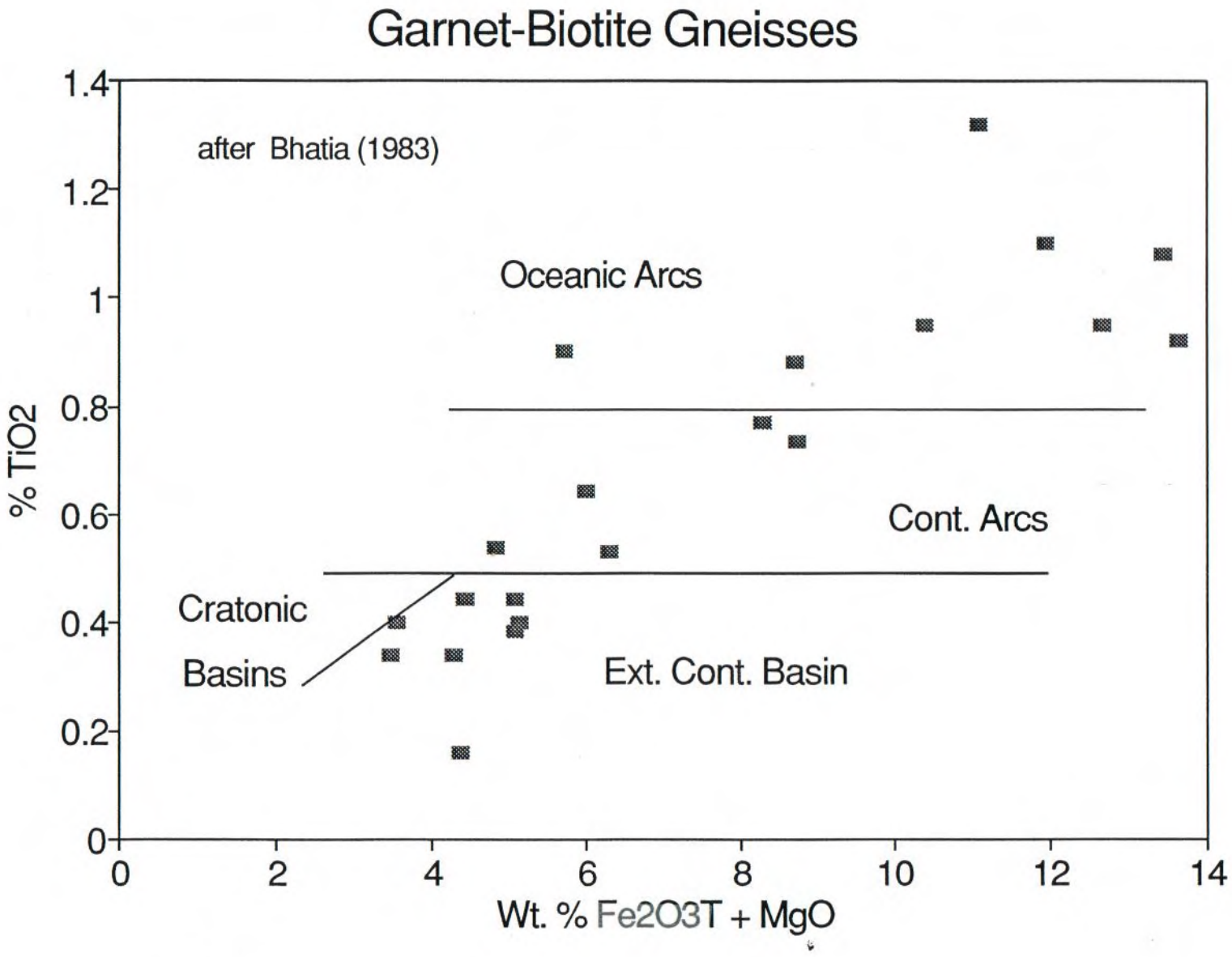
Garnet-Biotite Gneisses
after Bhatia (1983)
Oceanic Arcs
Cont. Arcs
Cratonic
Basins
Ext. Cont. Basin
% TiO2
Wt. % Fe2O3T + MgO
0
0.2
0.4
0.6
0.8
1
1.2
1.4
0
2
4
6
8
10
12
14

Figure 6.

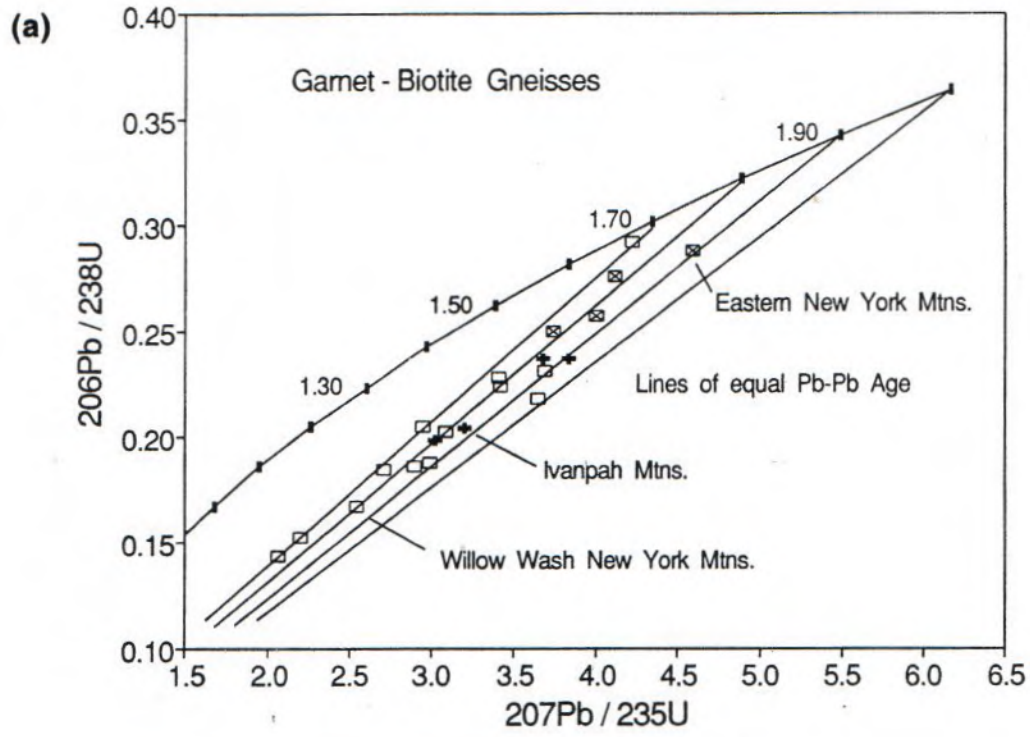
(a)
Garnet - Biotite Gneisses
1.90
1.70
1.50
1.30
Eastern New York Mtns.
Lines of equal Pb-Pb Age
Ivanpah Mtns.
Willow Wash New York Mtns.
206Pb / 238U
207Pb / 235U
0.40
0.35
0.30
0.25
0.20
0.15
0.10
1.5 2.0 2.5 3.0 3.5 4.0 4.5 5.0 5.5 6.0 6.5

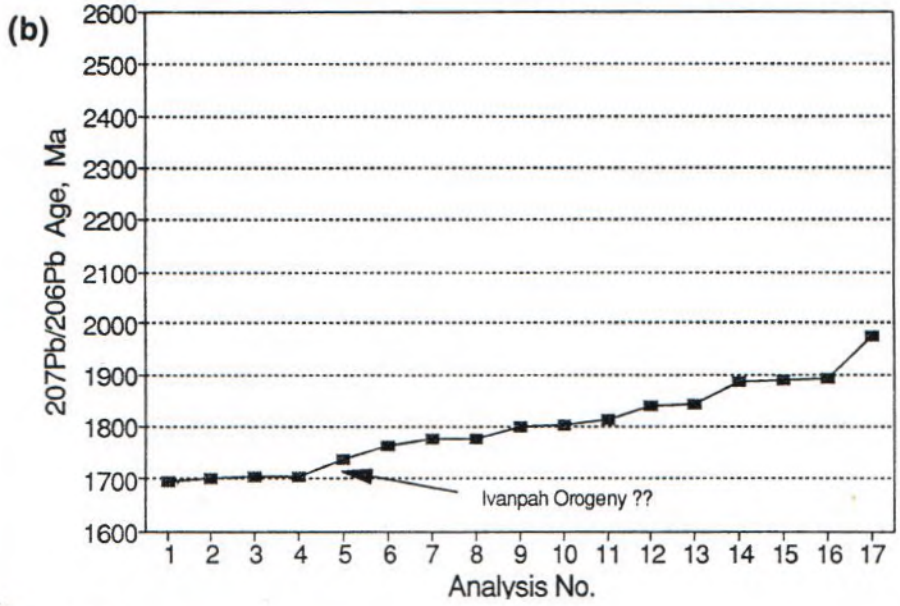
(b)
207Pb/206Pb Age, Ma
Ivanpah Orogeny ??
Analysis No.
2600
2500
2400
2300
2200
2100
2000
1900
1800
1700
1600
1 2 3 4 5 6 7 8 9 10 11 12 13 14 15 16 17

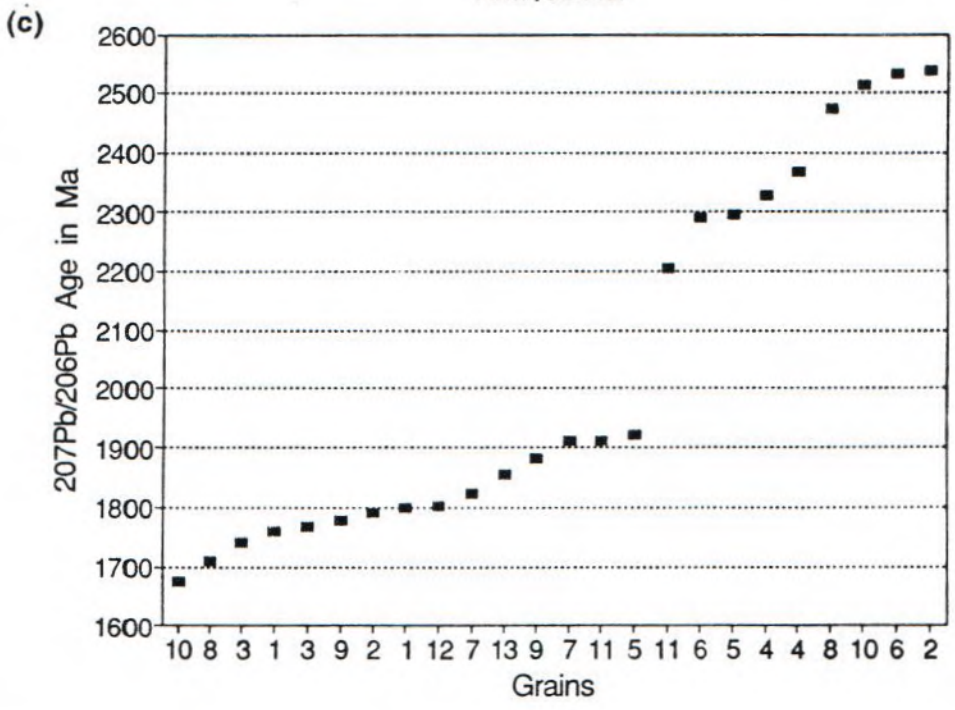
(c)
207Pb/206Pb Age in Ma
Grains
2600
2500
2400
2300
2200
2100
2000
1900
1800
1700
1600
10 8 3 1 3 9 2 1 12 7 13 9 7 11 5 11 6 5 4 4 8 10 6 2

Figure 7.

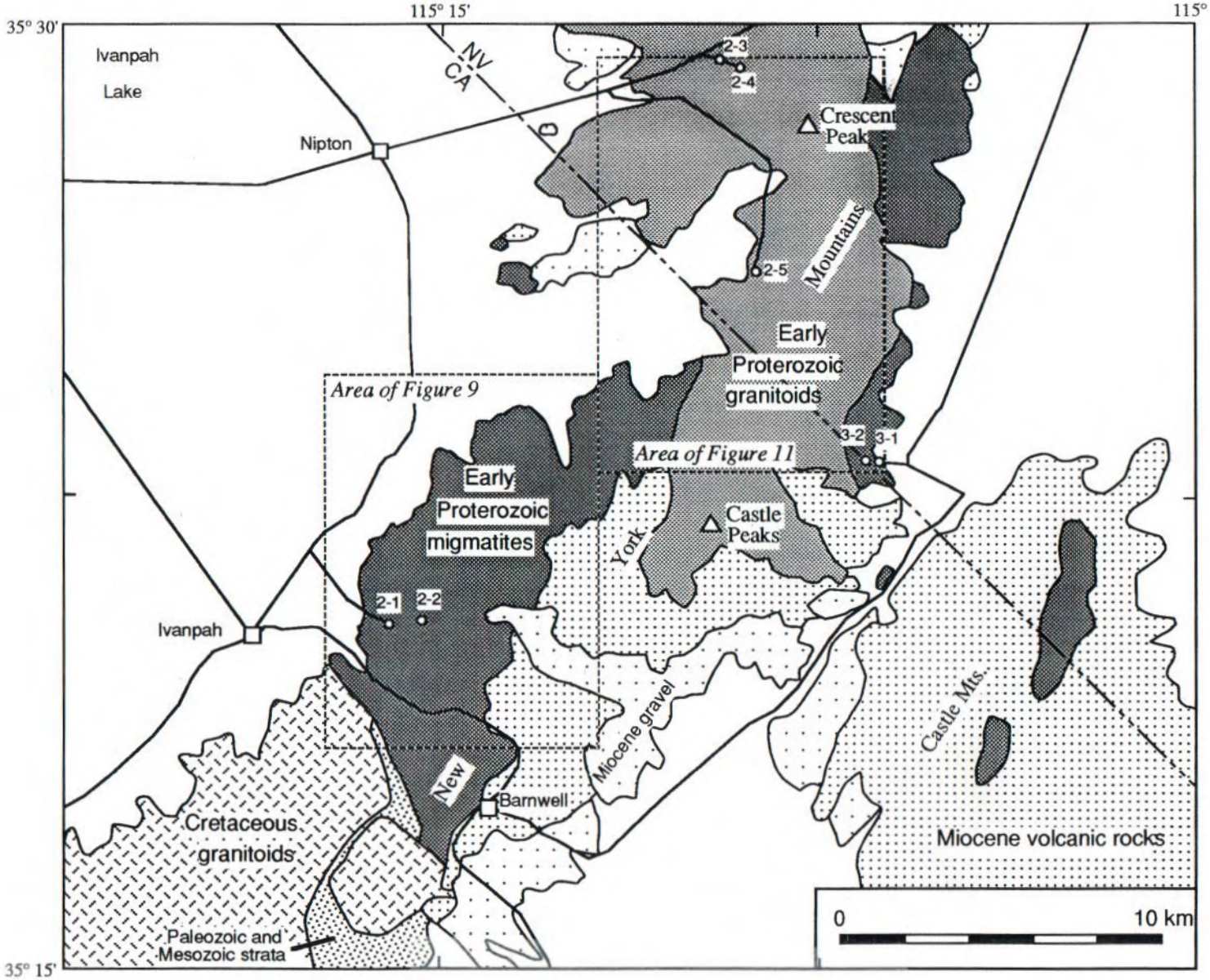
115° 15'
115°
35° 30'
35° 15'
Ivanpah
Lake
NV
CA
Nipton
2-3
2-4
Crescent
Peak
Mountains
2-5
Early
Proterozoic
granitoids
Area of Figure 9
3-2
3-1
Area of Figure 11
Early
Proterozoic
migmatites
Castle
Peaks
York
2-1
2-2
Ivanpah
Miocene gravel
Castle Mts.
New
Barnwell
Cretaceous
granitoids
Miocene volcanic rocks
Paleozoic and
Mesozoic strata
0
10 km

Figure 8.

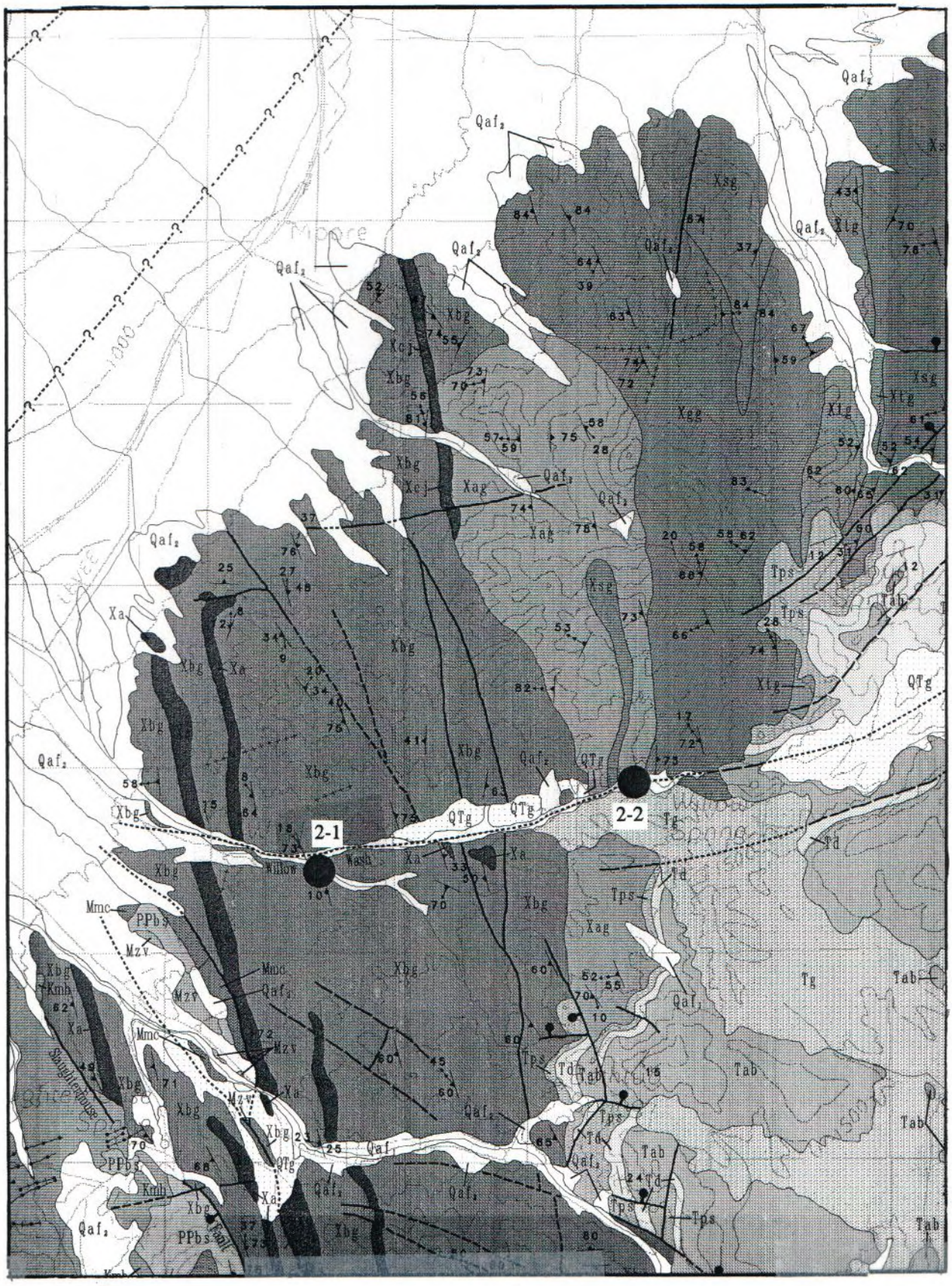
2-1
2-2
Qaf2
Qaf3
Xbg
Xcj
Xag
Xsg
Xtg
Xeg
Xa
QTg
Tps
Tab
Tg
Td
Mmc
PPbs
Mzv
Kmh
Qaf1

Figure 9.

CORRELATION OF MAP UNITS

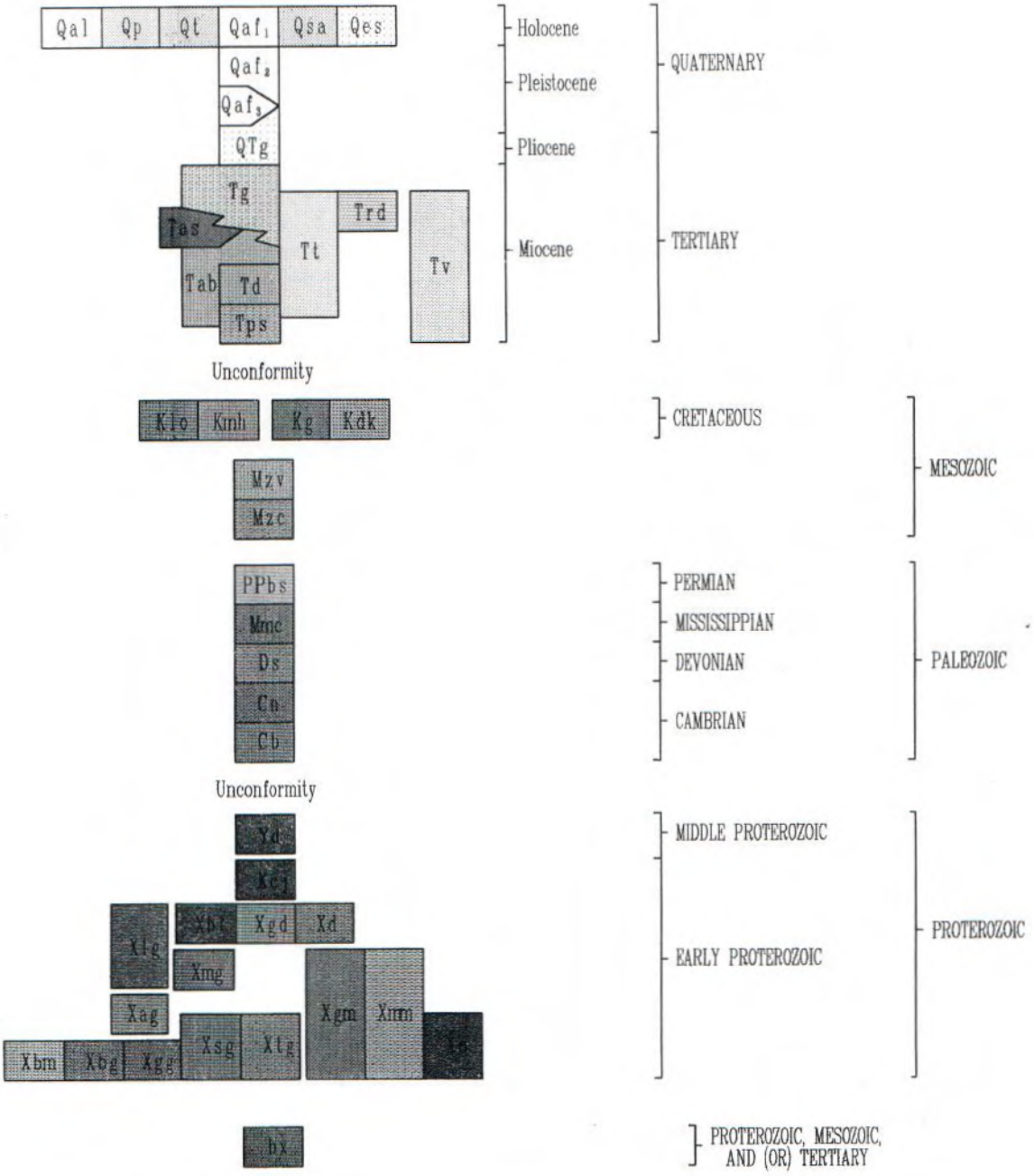

Figure 9 (continued).

DESCRIPTION OF MAP UNITS, Figures 9 and 11

Qaf_1 **Alluvial fan deposits** (Holocene)--Poorly sorted gravel, sand, and silt

Qaf_2 **Alluvial fan deposits** (Pleistocene)--Poorly sorted gravel, sand, and silt. Deposits typically underlie raised surfaces

QTg **Gravel** (Pleistocene and Pliocene)--Moderately consolidated alluvial deposits; typically underlies highly incised surfaces

Tg **Gravel** (Miocene)--Fluvial boulder- to pebble-gravel and sand interbedded with debris flows deposits and avalanche breccia

Tab **Andesite and basalt** (Miocene)--Lava flows and breccia composed of hornblende-pyroxene andesite and andesitic basalt

Td **Dacite** (Miocene)--Dacite to andesite breccia, domes, and lava flows

Tps **Peach Springs Tuff** of Young and Brennan (1974) (Miocene)--Welded rhyolite ash-flow tuff

Kmh **Mid Hills Adamellite** of Beckerman and others (1982) (Cretaceous)--Medium- to coarse-grained, porphyritic to equigranular, leucocratic monzogranite. Dated as about 93 Ma by U-Pb on zircon (Miller and others, 1994)

Kg **Granodiorite** (Cretaceous)--Biotite granodiorite and intrusion breccia at and west of Crescent Peak

Kdk **Dike swarms** (Cretaceous)--Leucocratic dikes present as swarm invading granodiorite southwest of townsite of Crescent

Mzv **Volcanic and sedimentary rocks** (Mesozoic)--Volcaniclastic rocks with lesser sedimentary rocks

Mzc **Calcsilicate rocks** (Mesozoic)--Metamorphosed calcsilicate rocks, tentatively correlated with the Moenkopi Formation (Burchfiel and Davis, 1977)

PPbs **Bird Spring Formation** (Permian and Pennsylvanian)--Thick-bedded cherty, sandy and pure limestone

Mmc **Monte Cristo Limestone** (Mississippian)--Massive pure, coarse limestone, cherty in lower part

Yd **Diabase** (Middle Proterozoic)--Dark colored, altered ophitic diabase

Xcj **Granodiorite of Crippled Jack Well** (Early Proterozoic)--Dark-colored, biotite-rich, hornblende-biotite granodiorite, commonly strongly porphyritic. About 1660 Ma.

Xd **Diorite** (Early Proterozoic)--Dark-brown to black hornblende diorite. Commonly strongly porphyritic

Xbt **Granodiorite of Big Tiger Wash** (Early Proterozoic)--Dark-brown, strongly porphyritic, biotite granodiorite. Encloses irregular patches of leucocratic granite. About 1675 Ma

Xgd **Granodiorite** (Early Proterozoic)--Dark-brown, subequigranular, biotite granodiorite. Grades to granodiorite of Big Tiger Wash with increasing content of potassium feldspar phenocrysts

Xlg **Leucocratic granite** (Early Proterozoic)--Light tan to white, subequigranular, leucocratic biotite granite. About 1672 Ma where associated with granodiorite of Big Tiger Wash; as old as 1695 along crest of New York Mountains (Wooden and Miller, 1990)

Xmg **Mesocratic granite** (Early Proterozoic)--Gray, subequigranular, mesocratic biotite granite. Closely associated with leucocratic granite along crest of New York Mountains. Outcrops typically display swirl patterns of rock with varying amounts of biotite and fragments of wallrocks

Xgm **Granite and metamorphic rocks** (Early Proterozoic)--Interleaved leucocratic granite and wallrock gneiss along east side of New York Mountains. Granite more abundant than wallrock gneiss. Represents complexly intruded margin of plutonic complex

Xmm **Mixed metamorphic rocks and granite** (Early Proterozoic)--Migmatitic gneiss and interleaved leucocratic granite along east side of New York Mountains. Represents complexly intruded margin of plutonic complex

Xag **Augen gneiss** (Early Proterozoic)--Biotite augen gneiss of granite to granodiorite composition, about 1710 Ma (Wooden and Miller, 1990)

Xbm **Biotite-rich migmatite** (Early Proterozoic)--Biotite migmatite gneiss typically folded in complex fashion. Lies along east side of plutonic complex underlying the crest of the New York Mountains.

Sequence of Willow Wash--Highly metamorphosed, compositionally-layered rocks mostly of supracrustal protolith. All rocks are intruded by abundant garnet-bearing leucocratic dikes and lesser amphibolite dikes

Xbg **Biotite-garnet gneiss migmatite** (Early Proterozoic)--Migmatite sequence with large amount of equigranular biotite-garnet gneiss. Includes quartzo-feldspathic gneiss, minor pelitic biotite-sillimanite-alkali feldspar gneiss

Xgg **Granitoid gneiss and migmatite** (Early Proterozoic)--Quartzo-feldspathic migmatite sequence with large amount of equigranular biotite granitoid gneiss. Includes quartzo-feldspathic gneiss

Xsg **Schistose gneiss and metaplutonic migmatite** (Early Proterozoic)--Migmatite sequence with large amount of schistose biotite-rich gneiss and granitoid gneisses of plutonic origin

Xtg **Tonalitic gneiss** (Early Proterozoic)--Migmatite sequence with large amount of equigranular biotite and hornblende-biotite tonalitic gneiss. Includes quartzo-feldspathic gneiss

Xa **Amphibolite** (Early Proterozoic)--Massive amphibolite and layered amphibolite gneiss containing amphibole, pyroxene, garnet, and biotite in varying ratios. Includes granulite facies mafic rock containing orthopyroxene

Figure 9 (continued).

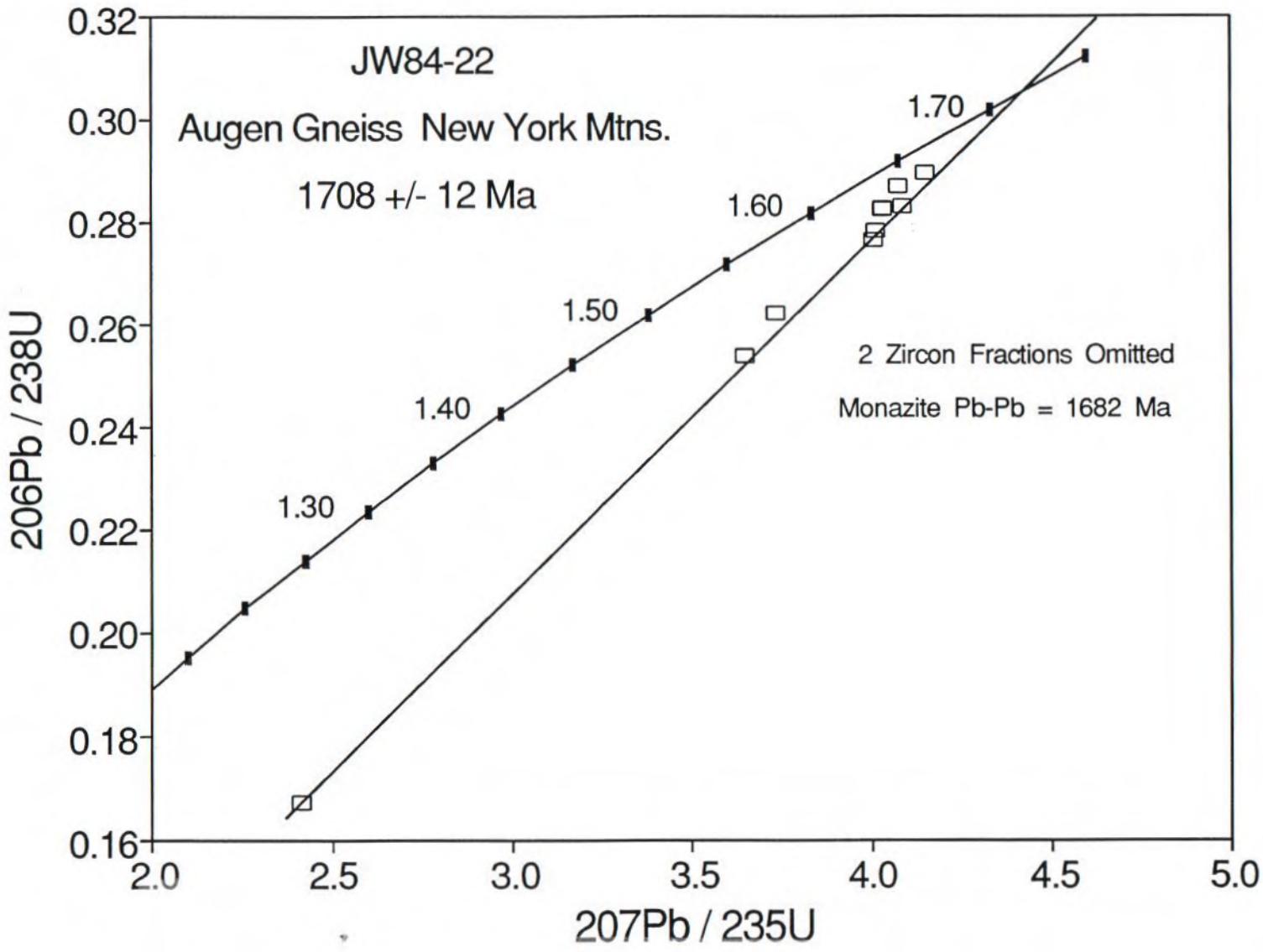
JW84-22
Augen Gneiss New York Mtns.
1708 +/- 12 Ma
1.70
1.60
1.50
1.40
1.30
2 Zircon Fractions Omitted
Monazite Pb-Pb = 1682 Ma
206Pb / 238U
207Pb / 235U
0.32
0.30
0.28
0.26
0.24
0.22
0.20
0.18
0.16
2.0
2.5
3.0
3.5
4.0
4.5
5.0

Figure 10.


2-3
2-4
2-5
3-2
3-1
Crescent Peak
Wash
QTg
Tg
Tab
Xcj
Xlg
Xmg
Xgm
Xgd
Xsg
Xd
Kg
Kdx
Xb
Ta
Qaf1
Qaf2
Qaf3

Figure 11.

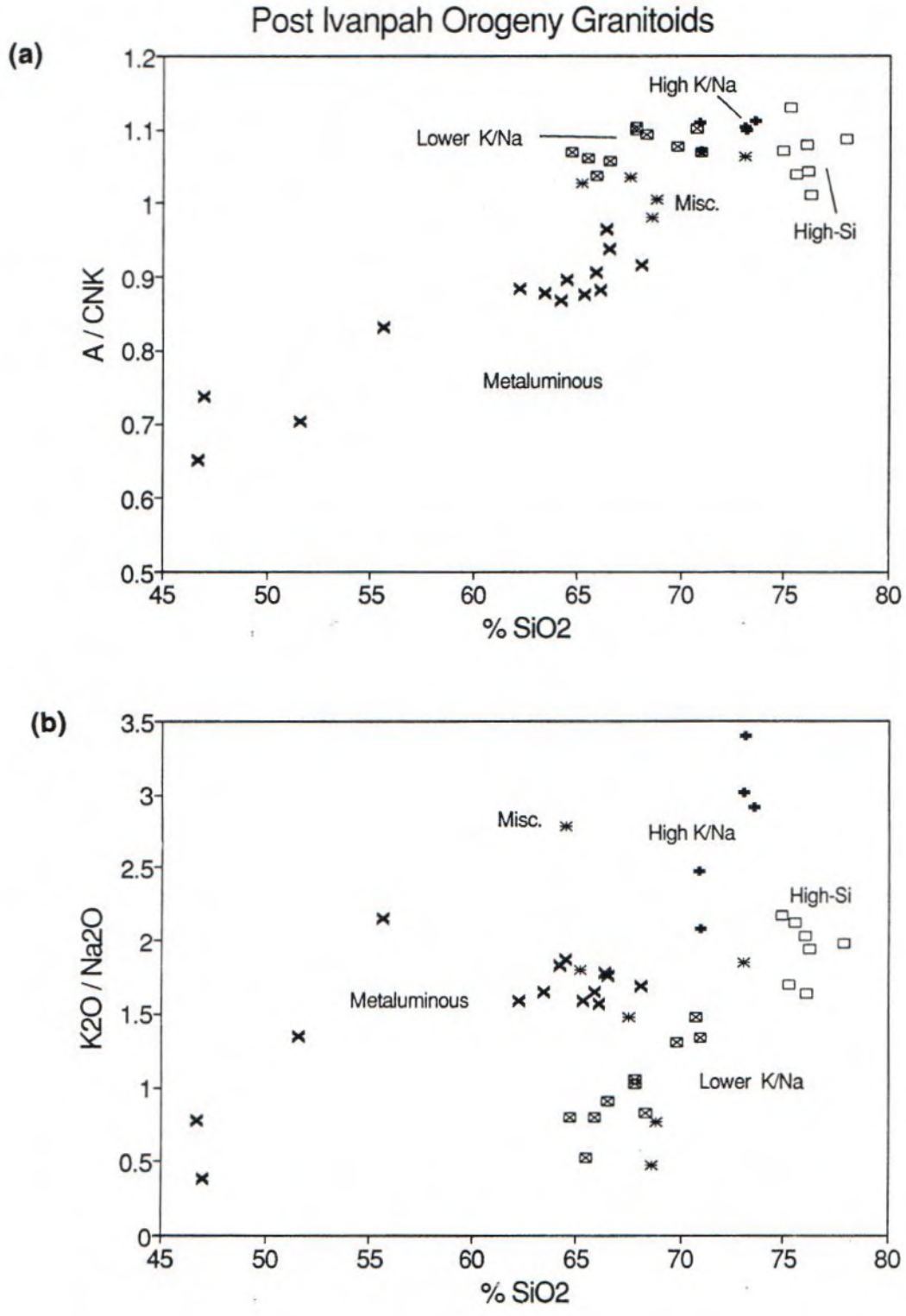
Post Ivanpah Orogeny Granitoids
(a)
A / CNK
% SiO2
High K/Na
Lower K/Na
Misc.
High-Si
Metaluminous
(b)
K2O / Na2O
% SiO2
Misc.
High K/Na
High-Si
Metaluminous
Lower K/Na

Figure 12.

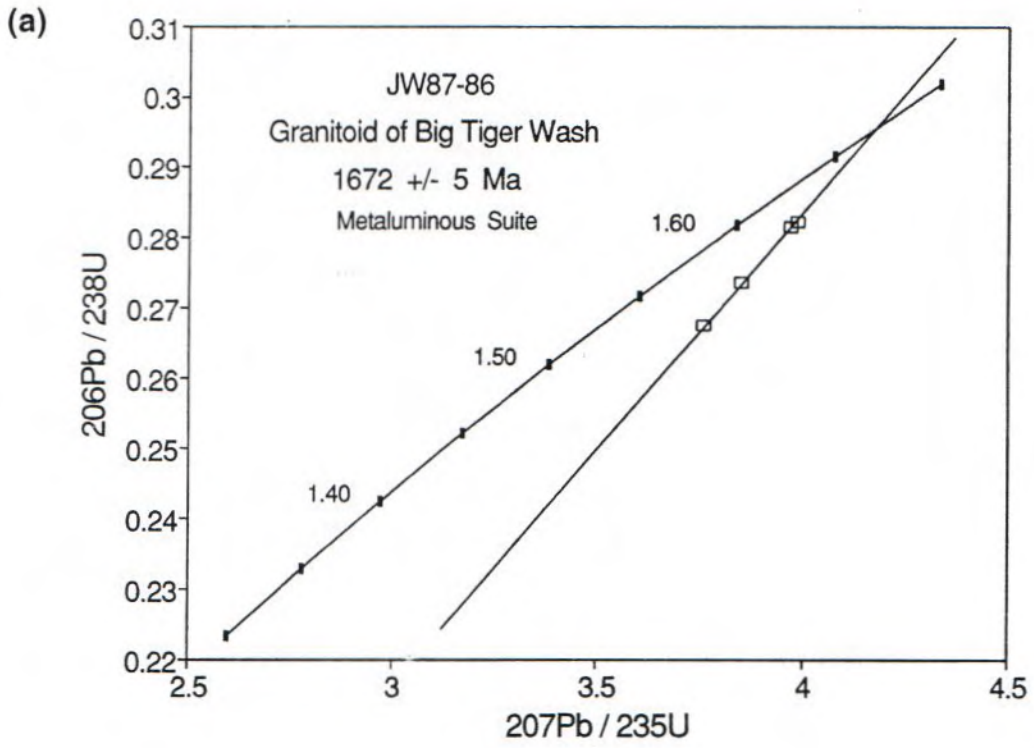
(a)
JW87-86
Granitoid of Big Tiger Wash
1672 +/- 5 Ma
Metaluminous Suite
1.60
1.50
1.40
206Pb / 238U
207Pb / 235U
0.31
0.3
0.29
0.28
0.27
0.26
0.25
0.24
0.23
0.22
2.5
3
3.5
4
4.5

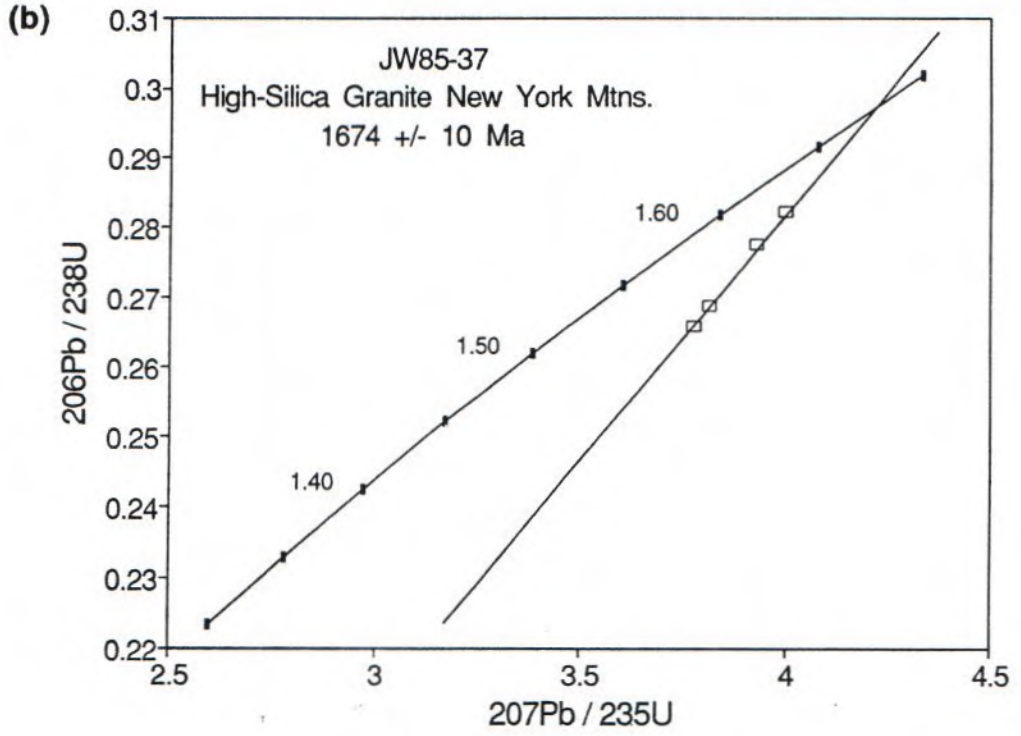
(b)
JW85-37
High-Silica Granite New York Mtns.
1674 +/- 10 Ma
1.60
1.50
1.40
206Pb / 238U
207Pb / 235U
0.31
0.3
0.29
0.28
0.27
0.26
0.25
0.24
0.23
0.22
2.5
3
3.5
4
4.5

Figure 13.

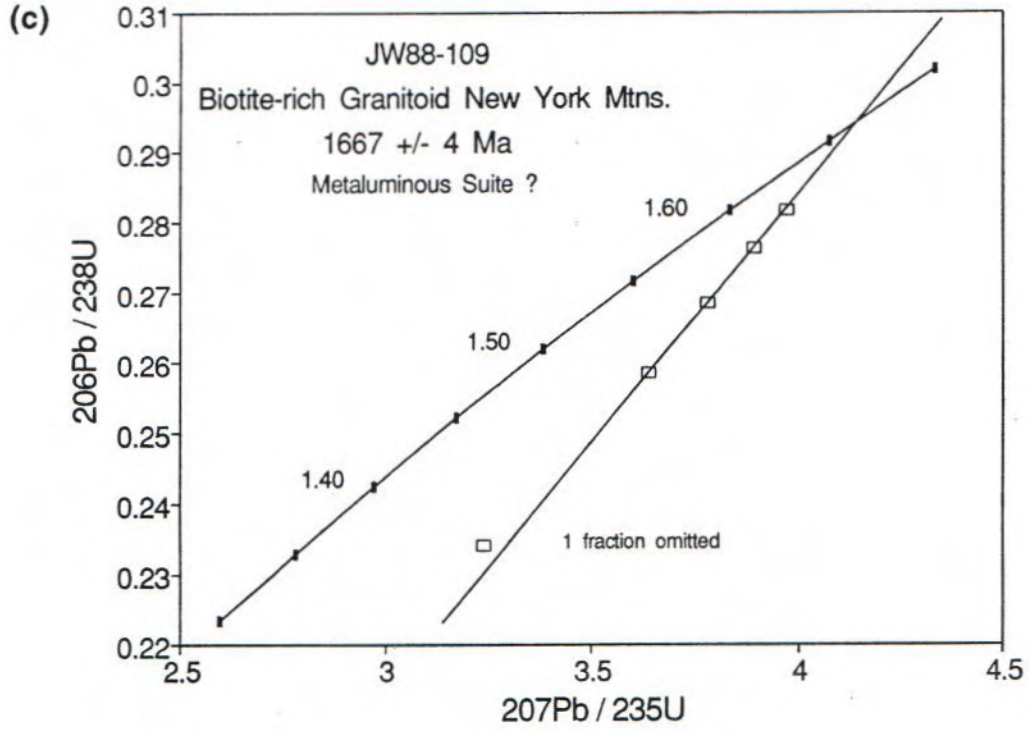

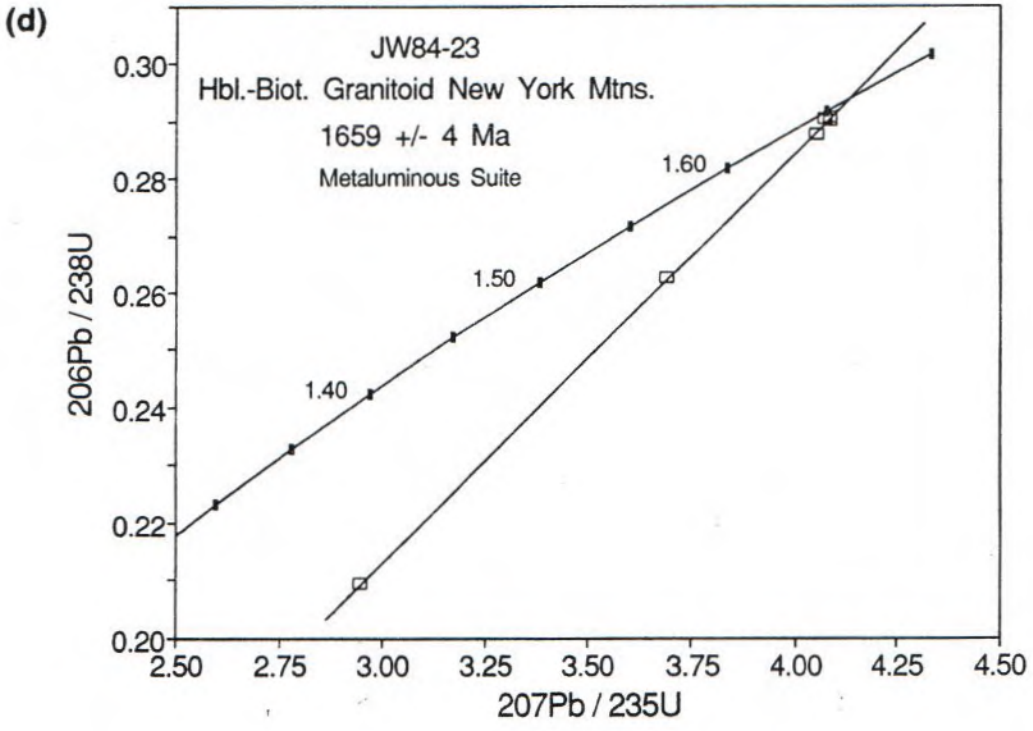

Figure 13 continued.

A

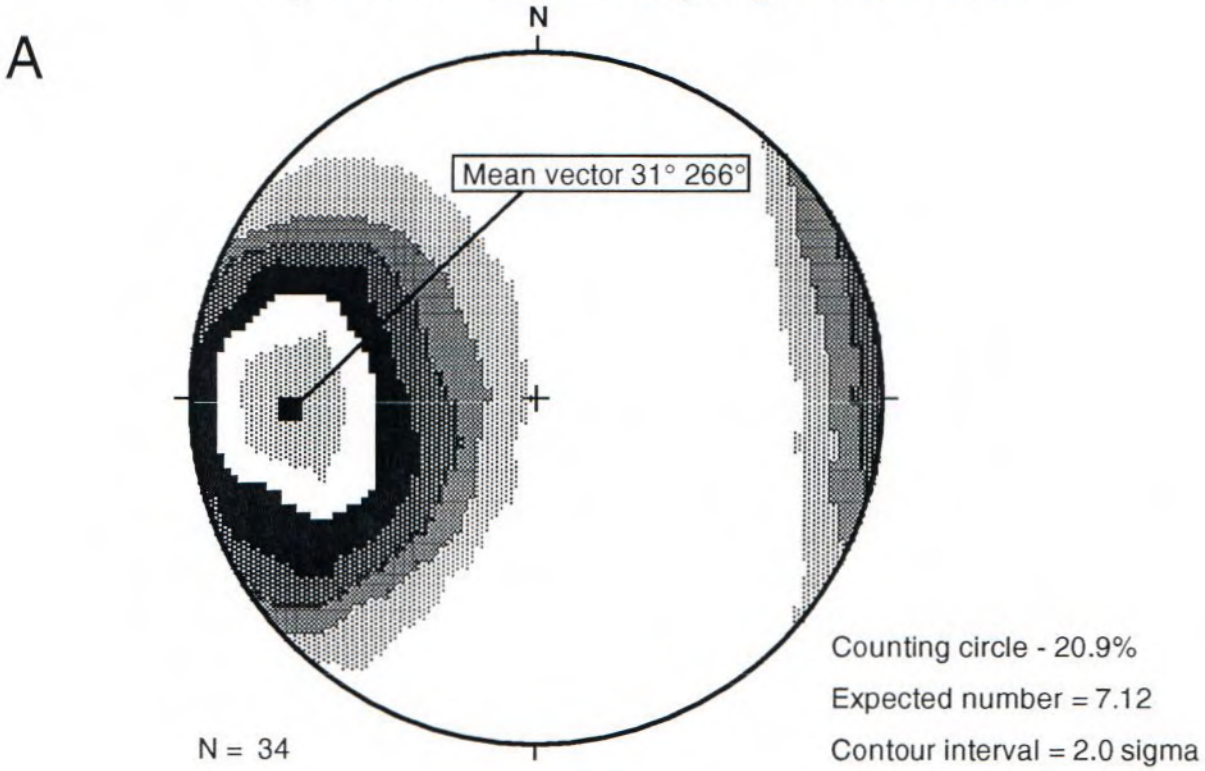
Mylonitic lineations, Big Tiger Wash area
N
Mean vector 31° 266°
N = 34
Counting circle - 20.9%
Expected number = 7.12
Contour interval = 2.0 sigma

B

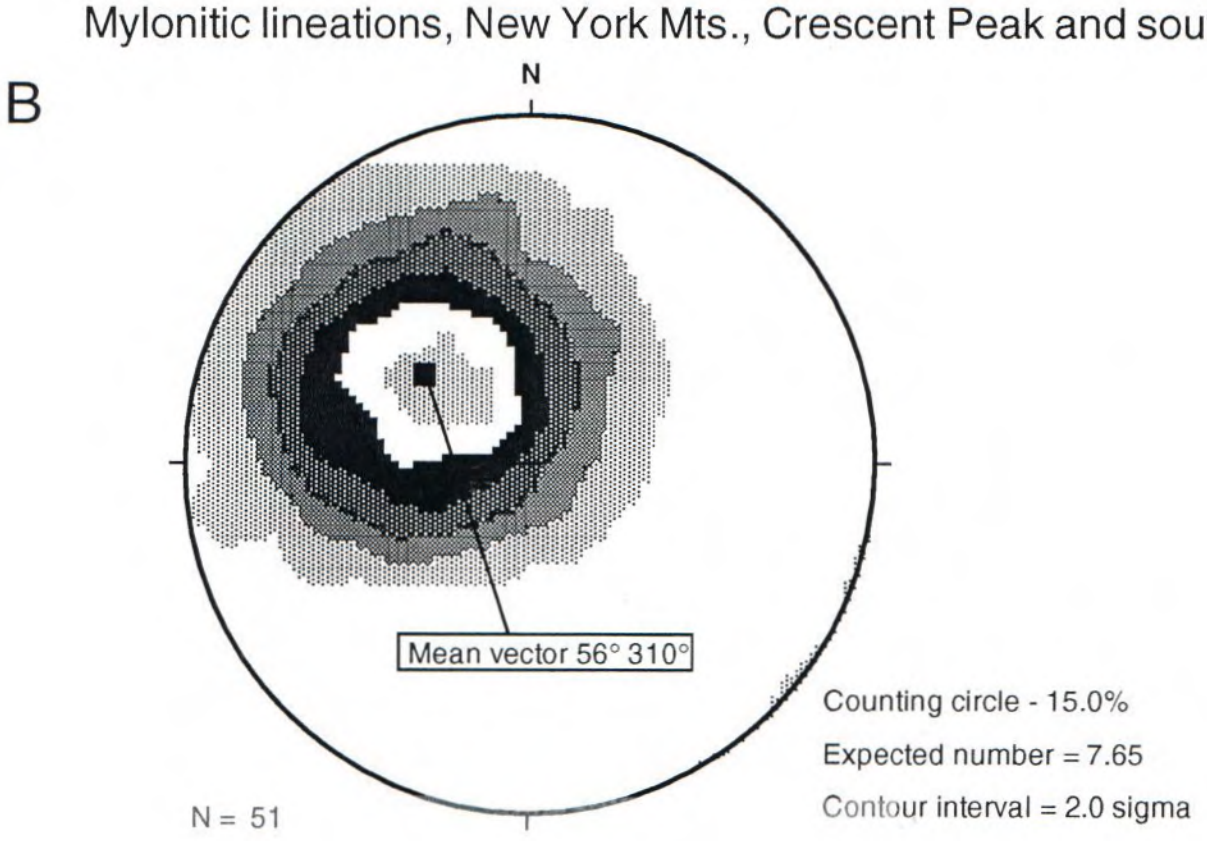
Mylonitic lineations, New York Mts., Crescent Peak and south
N
Mean vector 56° 310°
N = 51
Counting circle - 15.0%
Expected number = 7.65
Contour interval = 2.0 sigma

Figure 14.

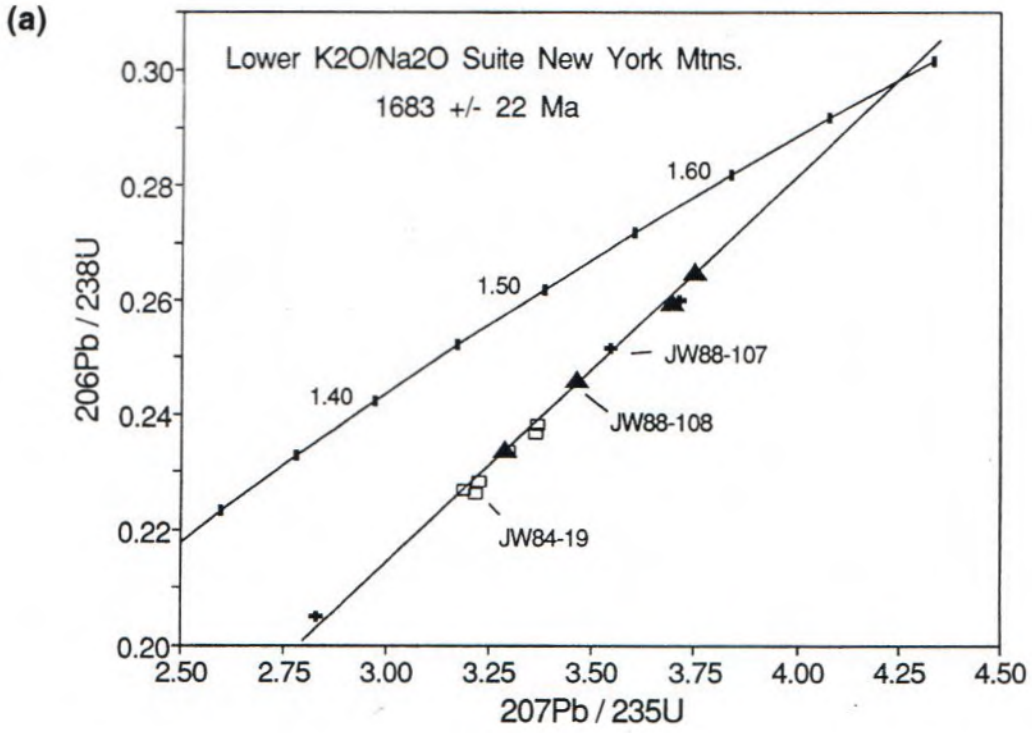
(a)
Lower K2O/Na2O Suite New York Mtns.
1683 +/- 22 Ma
1.60
1.50
1.40
JW88-107
JW88-108
JW84-19
206Pb / 238U
207Pb / 235U
0.30
0.28
0.26
0.24
0.22
0.20
2.50
2.75
3.00
3.25
3.50
3.75
4.00
4.25
4.50

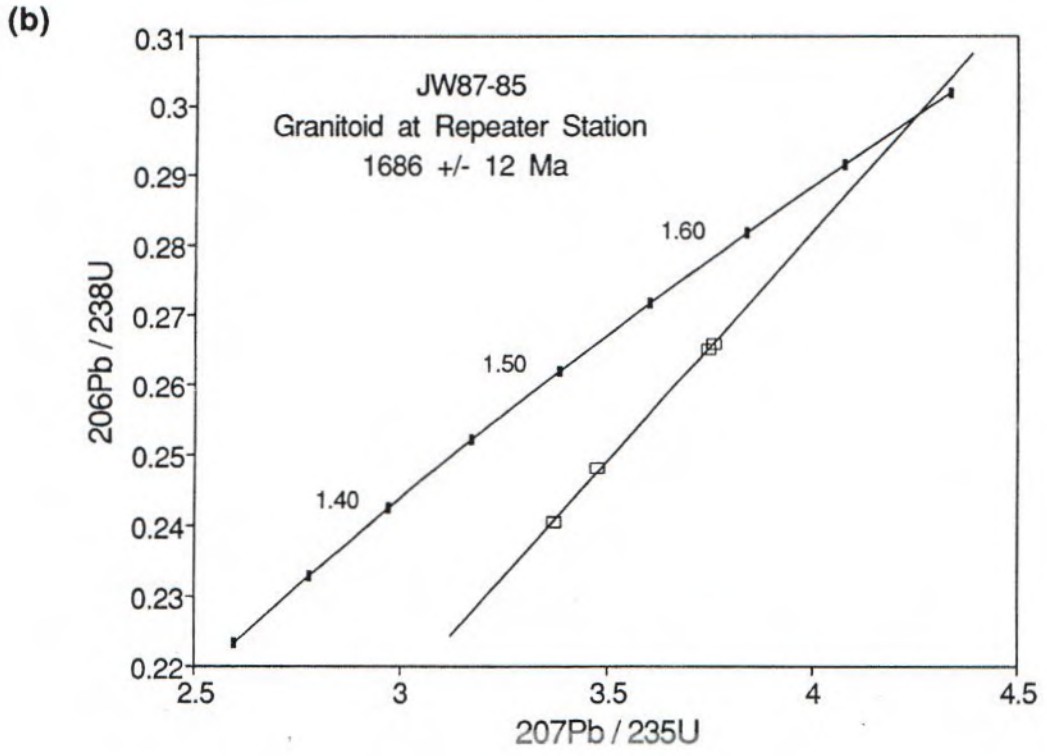
(b)
JW87-85
Granitoid at Repeater Station
1686 +/- 12 Ma
1.60
1.50
1.40
206Pb / 238U
207Pb / 235U
0.31
0.3
0.29
0.28
0.27
0.26
0.25
0.24
0.23
0.22
2.5
3
3.5
4
4.5

Figure 15.

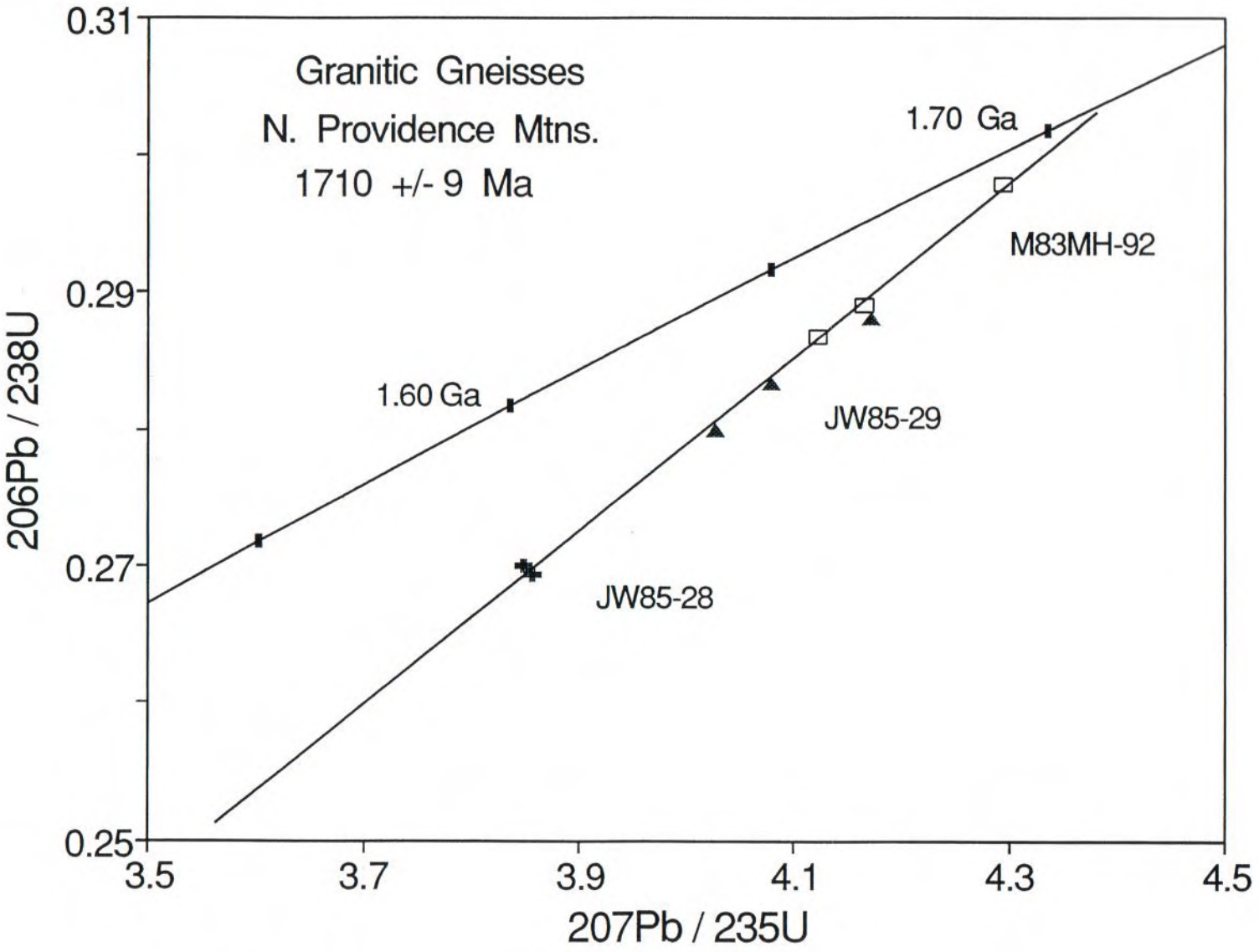
Granitic Gneisses
N. Providence Mtns.
1710 +/- 9 Ma
1.70 Ga
1.60 Ga
M83MH-92
JW85-29
JW85-28
0.31
0.29
0.27
0.25
206Pb / 238U
3.5
3.7
3.9
4.1
4.3
4.5
207Pb / 235U

Figure 16.

Table 1a

Representative Analyses of Metaigneous Gneisses - Ivanpah Mountains

	Gabbro	Quartz Diorite			Granodioritic Gneiss			Pawprint Gneiss		Trondhjemitic Gn.		Sodic Gneiss			Granitic Augen Gn
Sample	M88IV-51	M88 IV-52B	M89IV-03	M90IV-64	M90IV-55	M90IV-61	M90IV-63	JW89-146	M88IV-71	M90IV-45	M90IV-47	M90IV-73	M91IV-92	M91IV-93	M84IV-74
SiO2	50.40	59.10	56.00	65.70	67.70	65.70	66.00	67.1	71.90	69.90	69.70	68.40	65.9	61.8	70.5
TiO2	0.66	1.10	1.39	0.86	0.50	0.77	0.76	0.72	0.20	0.19	0.16	0.48	0.49	0.51	0.38
Al2O3	15.90	16.60	17.80	16.40	15.50	15.70	15.60	15.8	15.30	16.40	17.20	15.40	16.8	17.2	14.3
Fe2O3	1.15	2.88	2.09	1.00	0.79	1.21	0.93	1.10	0.52	0.59	0.25	0.84	1.37	2.48	0.77
FeO	6.91	5.14	7.37	3.92	3.24	4.49	4.41	3.66	1.53	1.31	0.88	2.45	2.67	2.92	2.01
MnO	0.13	0.12	0.12	0.04	0.05	0.06	0.05	0.03	0.04	0.02	0.02	0.04	0.05	0.09	0.02
MgO	9.20	1.80	2.38	1.94	1.75	1.34	1.34	1.19	0.45	1.10	0.75	0.98	1.62	2.44	0.54
CaO	11.20	6.50	6.60	4.33	5.14	4.35	4.19	3.06	2.36	3.48	4.09	3.08	4.36	5.72	1.72
Na2O	2.10	3.40	3.80	2.83	2.64	2.98	2.91	2.84	4.40	4.59	4.65	3.81	3.87	4.07	2.49
K2O	0.40	0.98	1.27	1.82	1.35	1.65	1.96	3.29	1.98	1.30	1.13	3.00	1.57	1.64	5.65
P2O5	0.12	0.56	0.57	0.05	0.16	0.34	0.34	0.17	0.10	0.10	0.09	0.16	0.16	0.25	0.15
CO2	0.03	0.07	1.00	0.01	0.02	0.01	0.01	0.03	0.02	0.03	0.01	0.05	0.11	0.10	0.10
H2O+	0.6	0.6	0.56	0.54	0.42	0.53	0.49	0.35	0.22	0.47	0.29	0.51	0.76	0.60	0.58
H2O-	0.08	0.09	0.11	0.08	0.12	0.09	0.13	0.12	0.05	0.10	0.07	0.06	0.09	0.05	0.05
TOTAL	98.88	98.94	101.06	99.52	99.38	99.22	99.12	99.46	99.07	99.58	99.29	99.26	99.82	99.87	99.26
Fe2O3T	8.75	8.53	10.20	5.35	4.39	6.19	5.83	5.13	2.22	2.04	1.23	3.56	4.33	5.72	2.98
ppm															
Nb			10	<10	<10	14	<10	14	10	<10	<10	<10	<10	<10	10
Rb	<10	18	26	62	54	80	62	114	30	54	38	108	91	64	143
Sr	215	240	220	230	192	205	180	160	205	360	470	305	455	550	107
Zr	62	530	830	285	260	600	435	690	230	102	196	355	154	158	199
Y	14	34	36	26	18	28	18	36	12	<10	<10	20	10	28	35
Ba	152	750	890	305	350	850	740	1800	610	310	295	800	620	300	1050
K2O/Na2O	0.19	0.29	0.33	0.64	0.51	0.55	0.67	1.16	0.45	0.28	0.24	0.79	0.41	0.40	2.27
A/CNK	0.66	0.90	0.91	1.13	1.02	1.08	1.07	1.15	1.12	1.07	1.05	1.02	1.05	0.91	1.07

Table 1b

Representative Trace Element Analyses of Metaigneous Gneisses - Ivanpah Mountains

	Gabbro	Mafic Tonalite		Granodioritic Gneiss				Pawprint Gneiss		Trondhjemitic Gneiss		Sodic Gneiss		Granitic Augen Gneiss
*	---------	******	******	+++++	+++++	+++++	+++++	=====	=====	######	######	******	******	=====
Sample	M88IV-51	M88IV-52B	M89IV-3	M90IV-64	M90IV-55	M90IV-61	M90IV-63	JW89-146	M88IV-71	M90IV-45	M90IV-47	M90IV-73	M88IV-72	M84IV-74
Sc	32	23	27	10	12	14	13	9	4	4	2	7	1	6
Cr	657	31	26	52	40	18	14	14	3	12	14	9	5	10
Co	45	17	21	15	12	12	11	9	3	6	4	7	3	5
Ni	204	71	25	24	12	12		15		9	7			
Zn	82	104	124	94	62	58	66	70	27	37	27	63	20	23
Rb	<8	33	39	80	60	88	74	113	40	71	37	118	30	143
Cs	<0.2	0.34	0.26	1.36	1.1	1.2	0.74	0.71	0.27	1.6	0.94	4.9	0.35	0.43
Ba	133	890	930	338	374	892	747	1560	521	272	267	793	187	1050
La	10.7	34.5	44.8	102	13.6	41.5	20.6	169	35.6	8.82	12	45.7	9.35	48.6
Ce	24.2	69.5	97.1	205	26.3	85.8	49.7	361	58.2	17.6	22.8	91.7	16.2	101
Nd	11.6	32	44.1	77.9	11.7	36.4	27.1	128	20.7	8.28	9.41	35.2	5.9	39.5
Sm	3.18	7.15	8.97	10.9	2.58	6.57	6.13	20.1	3.58	1.67	1.76	5.8	1.14	6.85
Eu	0.85	2.26	2.34	1.93	1.09	1.95	1.44	1.96	0.9	0.46	0.64	1.13	0.59	1.15
Tb	0.49	0.9	0.98	1	0.27	0.73	0.65	1.5	0.39	0.155	0.129	0.45	0.06	0.83
Yb	1.47	2.62	2.85	1.56	0.52	1.57	1.12	2.26	1.25	0.311	0.221	0.83		5.77
Lu	0.205	0.4	0.42	0.21	0.073	0.24	0.15	0.32	0.16	0.04	0.032	0.114	0.01	0.88
Hf	2.23	13.5	18.8	7.6	6.3	14	11	14.9	3.16	2.29	3.38	5.7	1.62	6.13
Ta	0.21	0.95	0.82	0.4	0.3	0.54	0.49	0.52	0.27	0.076	0.245	0.54	0.17	0.3
Th	0.3	1.45	1.8	27.1	0.24	4.32	0.91	55	11.9	3.34	5.06	12.5	0.29	20.4
U	<0.3	1.03	0.88	1.45	0.64	0.88	0.78	3.9	1.8	1.22	0.98	1.3	0.3	1
Nb						14		14	10					
Sr	215	240	220	230	192	205	180	160	205	360	470	305	315	107
Zr	62	530	830	285	260	600	435	690	230	102	196	355	142	206
Y	14	34	36	26	18	28	18	36	12			20		35
Sample/Chondrites														
La	34.6	111.7	145.0	330.1	44.0	134.3	66.7	546.9	115.2	28.5	38.8	147.9	30.3	157.3
Ce	30.0	86.1	120.3	254.0	32.6	106.3	61.6	447.3	72.1	21.8	28.3	113.6	20.1	125.2
Nd	19.4	53.4	73.6	130.1	19.5	60.8	45.2	213.7	34.6	13.8	15.7	58.8	9.8	65.9
Sm	16.3	36.7	46.0	55.9	13.2	33.7	31.4	103.1	18.4	8.6	9.0	29.7	5.8	35.1
Eu	11.6	31.0	32.1	26.4	14.9	26.7	19.7	26.8	12.3	6.3	8.8	15.5	8.1	15.8
Tb	10.4	19.1	20.9	21.3	5.7	15.5	13.8	31.9	8.3	3.3	2.7	9.6	1.3	17.7
Yb	7.1	12.6	13.7	7.5	2.5	7.5	5.4	10.9	6.0	1.5	1.1	4.0		27.7

Table 2a

Representative Analyses of Metasedimentary Rocks and Amphibolites - Ivanpah Mountains

	Biotite-Garnet Gneiss					Pelitic Gneiss				Amphibolite					
	---------	---------	---------	---------	---------	******	******	******	******	######	######	######	######	######	######
Sample	JW86-79	M87IV-23	M87IV-19	M87IV-17	M91IV-101	M88IV-74	M88IV-75	M90IV-57	M90IV-69	M87IV-12 dike	M88IV-53 dike	88IV-69	M90IV-49	M90IV-54	M90IV-58
SiO2	61.20	62.70	66.00	68.40	75.8	55.80	58.70	61.70	74.80	47.5	47.4	48.60	50.4	52.4	48.6
TiO2	1.10	1.32	0.64	0.16	0.56	1.00	0.86	0.94	0.67	0.38	0.62	1.14	0.2	1.8	0.87
Al2O3	16.20	15.50	16.70	15.60	11.8	23.90	22.40	19.20	11.40	6.66	14.5	14.80	19.7	14.8	13.7
Fe2O3T	8.96	9.50	4.39	2.98	3.87	8.84	7.55	9.91	4.68	9.63	11.3	13.30	6.65	16.3	12.8
Fe2O3					0.48	4.17	2.53	1.15	0.60	1.52	2.18	4.84	1.48	1.89	1.36
FeO					3.05	4.21	4.52	7.89	3.68	7.37	8.29	7.69	4.7	13.1	10.4
MnO	0.09	0.12	0.04	0.05	0.05	0.14	0.11	0.23	0.03	0.17	0.19	0.19	0.12	0.21	0.21
MgO	3.00	1.60	1.60	1.40	1.07	2.50	2.10	2.61	2.05	18.5	9.5	7.20	6.61	5.15	9.14
CaO	4.16	3.98	4.38	4.60	2.5	0.76	0.70	0.65	0.80	13.9	11.5	9.88	13.5	8.14	10.8
Na2O	2.60	2.10	3.60	3.10	2.71	1.20	1.20	0.72	1.22	1.3	2.5	2.00	2.55	0.23	0.59
K2O	1.54	1.78	1.32	1.48	1.07	3.62	4.10	3.48	2.93	0.24	0.72	1.08	0.27	0.7	1.3
P2O5	0.16	0.50	0.24	0.10	0.13	0.06	0.06	0.07	0.06	0.1	0.36	0.16	-0.05	0.15	0.3
CO2					0.05	0.06	0.13	0.09	0.14	0.01	0.07	0.08	0.05	0.08	0.12
H2O+	0.38	1.25	0.75	2.25	0.38	1.85	1.50	0.67	0.70	0.78	0.25	0.19	0.04	0.11	0.6
H2O-	(LOI)	(LOI)	(LOI)	(LOI)	0.06	0.21	0.15	0.09	0.05	1.19	1.11	1.87	0.84	0.97	2.06
TOTAL	99.39	100.35	99.66	100.12	99.71	99.48	99.06	99.49	99.13	99.62	99.19	99.72	100.41	99.73	100.05
ppm															
Nb					13	24	24	12	<10						
Rb					60	182	180	126	88		<10	34	12	32	52
Sr					205	86	110	106	102		102	230	104	205	120
Zr					315	315	330	375	405		36	60	10	94	66
Y					24	38	40	44	30		-10	20	10	32	22
Ba					245	880	1000	780	670		188	210	38	150	395
Ni					19	52	40	54	26		168	80	76	108	134
Cr						152	116	132	60		290	162	315	80	260
A/CNK	1.20	1.23	1.09	1.04	1.16	3.28	2.91	3.13	1.72						

Amp

Table 2b

Representative Trace Element Analyses of Metasedimentary Rocks and Amphibolites - Ivanpah Mountains

	Pelitic gneiss				Amphibolite				
	********	********	*********	********	########	########	########	########	########
Sample	M88IV-74	M88IV-75	M90IV-57	M90IV-69	M88IV-53	M88IV-69	M90IV-49	M90IV-54	M90IV-58
ppm									
Sc	27	26	26	11	40	39	33	26	45
Cr	131	111	116	69	279	152	327	89	238
Co	26	24	29	10	55	45	26	49	54
Ni	70	60	36	23	161	77	62	74	124
Zn	156	134	127	89	85	101	91	146	
Rb	205	212	152	100	17	51	6.5	38	51
Cs	4.82	4.19	2.35	0.91	-0.3	0.27	0.2	0.33	0.66
Ba	825	939	836	652	198	200	47	131	400
La	75.5	62.5	70.9	47.4	3.1	2.03	0.57	4.29	5.73
Ce	143.9	117.6	147	105	7.7	6.9	1.38	10.9	13.8
Nd	61.1	49.6	62.5	43.3	-6	6.8	1.17	10	8
Sm	11.8	9.93	10.7	8.12	1.52	2.49	0.474	4.56	2.38
Eu	1.55	1.64	1.48	1.19	0.58	0.88	0.33	1.42	0.79
Tb	1.53	1.4	1.18	0.83	0.44	0.64	0.151	0.92	0.49
Yb	4.74	5.03	4.49	2.3	1.66	2.64	0.85	2.86	2.12
Lu	0.69	0.72	0.65	0.35	0.26	0.39	0.13	0.42	0.36
Hf	7.08	4.2	6.76	7.76	1.06	1.49	0.19	2.52	1.47
Ta	1.01	0.96	0.74	0.51	0.21	0.17	0.025	0.17	0.27
Th	23	18.2	23	16.5	0.59	0.34	0.22	0.55	0.98
U	2.5	2.2	2.53	2.05	0.74	-0.3	0.19	0.4	0.52
Nb	24	24	12						
Sr	86	110	106	102	102	230	104	205	120
Zr	315	330	375	405	36	60	10	94	66
Y	38	40	44	30		20	10	32	22
Sample/Chondrites									
La	244.3	202.3	229.4	153.4	10.0	6.6	1.8	13.9	18.5
Ce	178.3	145.7	182.2	130.1	9.5	8.6	1.7	13.5	17.1
Nd	102.0	82.8	104.3	72.3		11.4	2.0	16.7	13.4
Sm	60.5	50.9	54.9	41.6	7.8	12.8	2.4	23.4	12.2
Eu	21.2	22.5	20.3	16.3	7.9	12.1	4.5	19.5	10.8
Tb	32.6	29.8	25.1	17.7	9.4	13.6	3.2	19.6	10.4
Yb	22.8	24.2	21.6	11.1	8.0	12.7	4.1	13.8	10.2

Table 3a

Representative Analyses of Metaigneous Rocks - Willow Wash and Vicinity, New York Mountains

	Garnet Leuco-granite	Pink Granite		Granitic Gneiss		Augen Gneiss		High-Al Amphibolite			Tholeiitic Amphibolite				High-Mg Amphibolite		
	######	******	******	=====	=====	+++++	+++++	*****	*****	*****	=====	=====	=====	=====	+++++	+++++	+++++
Sample	M84	JW85-27	JW85-30	JW85-9	M84	M84	M88	ENY-97	JW85-31	ENY-52	M86	M88	M88	M88	ENY-132	88-NY37	ENY-142
	NY-68B				NY-72	NY-77	NY-03A				NY-10A	NY-02B	NY-08	NY-22			
SiO2	74.30	74.60	77.20	69.90	72.20	68.60	65.60	49.00	47.50	45.40	48.80	48.00	48.00	53.60	43.20	46.80	49.60
TiO2	0.03	0.13	0.06	0.68	0.47	0.61	0.72	0.22	0.45	1.58	1.11	0.68	2.06	0.88	0.40	0.64	0.25
Al2O3	13.90	13.50	12.10	11.20	13.10	14.70	15.10	18.80	20.60	17.60	14.10	15.00	13.70	14.20	9.62	7.33	13.70
Fe2O3T	0.07	0.93	1.22	9.26	4.08	4.95	6.05	8.43	8.25	14.70	13.60	13.50	15.60	10.60	12.70	12.40	11.50
MnO	0.01	0.02	0.02	0.17	0.01	0.02	0.06	0.14	0.12	0.14	0.23	0.21	0.23	0.17	0.15	0.18	0.19
MgO	0.10	0.26	0.12	0.17	0.74	0.94	1.30	9.44	6.52	5.81	7.70	7.30	5.90	6.20	22.30	18.90	13.20
CaO	0.31	1.63	0.62	3.05	1.96	3.26	3.06	11.90	12.00	10.60	11.90	10.40	11.70	8.70	6.98	9.56	9.77
Na2O	2.08	2.76	2.51	2.30	2.46	3.45	3.50	1.41	2.44	2.51	1.53	1.50	0.65	0.90	1.04	1.30	1.10
K2O	8.26	5.33	5.92	2.97	4.19	2.27	1.70	0.24	0.89	0.40	0.59	0.54	0.40	1.44	0.18	0.42	0.29
P2O5	0.07	0.04	0.04	0.10	0.13	0.18	0.26	0.05	0.05	0.06	0.08	0.04	0.46	0.50	0.05	0.20	<.05
Fe2O3	0.03	0.30		3.88	0.67	1.19	1.64				3.22	3.95	5.60	1.92	4.54	6.20	1.81
FeO	0.05	0.57		4.89	3.10	3.42	3.97				9.44	8.68	9.09	7.89	7.42	5.64	8.81
CO2	0.09	0.08	0.06	0.07	0.02	0.13	0.13				0.12	0.22	0.04	0.36	0.66	0.16	0.25
H2O+	0.22	0.38	0.34	0.44	0.43	0.69	1.61				1.67	2.69	1.16	2.22	2.99	2.53	1.44
H2O-	0.03	0.04	0.03	0.06	0.04	0.07	0.08				0.12	0.21	0.11	0.13	0.09	0.07	0.07
LOI	0.36	0.60	0.39	0.35	0.19	0.68	1.70	0.93	1.79	1.26	0.93	2.39	0.55	1.80	2.19	1.76	1.44
TOTAL	99.49	99.80	100.20	100.15	99.53	99.66	99.05	100.56	100.61	100.06	100.61	99.42	99.10	99.11	99.62	99.93	100.48
A/CNK	1.08	1.02	1.04	0.89	1.08	1.05	1.15										
K2O/Na2O	3.97	1.93	2.36	1.29	1.70	0.66	0.49										
FeOT/MgO								0.80	1.14	2.28	1.59	1.66	2.38	1.54	0.51	0.59	0.78

Table 3b

Representative Analyses of Metasupracrustal Rocks - Willow Wash and Vicinity, New York Mountains

	Garnet-Biotite Gneiss										Pelitic Gneiss			Other Gneissic Rocks				
Sample	ENY-103	ENY-108	JW85-6	JW84-18	ENY-133	JW85-32	JW85-7	JW85-33	M88 NY-11A	M88 NY-39	ENY-145	ENY-146	M88 NY-11B	ENY-134	ENY-135	ENY-110	ENY-105	ENY-106
SiO2	59.40	60.80	62.70	63.70	64.20	66.50	68.50	70.20	71.30	71.10	59.40	62.70	70.00	72.00	76.00	79.50	83.40	90.60
TiO2	1.08	0.92	0.95	0.95	0.69	0.73	0.44	0.38	0.54	0.34	0.94	0.98	0.54	0.25	0.08	0.44	0.40	0.26
Al2O3	17.10	16.70	15.50	15.40	16.00	15.10	15.20	15.00	14.00	14.70	18.20	18.00	14.60	14.30	12.80	9.03	7.15	5.28
Fe2O3T	10.60	10.30	9.53	8.21	6.72	6.73	4.01	4.20	3.72	2.88	9.49	9.04	3.96	2.53	1.15	3.31	2.29	1.01
MnO	0.19	0.14	0.14	0.14	0.07	0.09	0.03	0.03	0.07	0.08	0.13	0.09	0.04	0.02	0.03	0.03	0.02	0.02
MgO	2.86	3.35	3.16	2.19	1.89	1.99	1.06	0.88	1.10	0.60	2.63	2.42	1.30	0.81	0.29	0.95	1.03	0.34
CaO	4.30	3.37	3.26	3.68	5.78	3.80	3.62	3.33	2.36	2.18	0.95	0.37	1.12	2.99	1.28	0.61	0.83	0.35
Na2O	2.49	2.22	2.20	2.61	3.18	2.83	3.76	3.92	3.10	3.10	1.58	0.52	2.30	3.04	2.19	1.44	0.96	0.65
K2O	1.93	1.90	2.09	1.98	0.70	1.68	1.35	1.23	1.48	3.96	5.19	4.07	4.30	3.29	5.70	3.89	2.63	1.05
P2O5	0.15	0.05	0.13	0.15	0.16	0.16	0.16	0.10	0.10	0.10	0.06	0.06	0.08	0.06	0.05	0.05	0.10	0.05
Fe2O3				1.03	2.12				0.63	0.59	2.92	2.90	0.91	0.79	0.24			
FeO				6.53	4.18				2.78	2.06	5.97	5.58	2.75	1.58	0.83			
CO2				0.03	0.37				0.05	0.01	0.45	0.06	0.07	0.12	0.16			
H2O+				0.70	1.10				1.21	0.48	1.50	2.43	1.23	0.59	0.37			
H2O-				0.07	0.10				0.33	0.02	0.24	0.32	0.23	0.01	0.02			
LOI	0.01	1.07	0.56	0.41	1.14	0.61	1.02	0.67	1.64	0.41	1.79	2.66	1.62	0.05	0.46	0.72	1.30	0.54
TOTAL	100.11	100.82	100.22	99.42	100.53	100.22	99.15	99.94	99.41	99.45	100.36	100.91	99.86	99.34	100.03	99.97	100.11	100.15
A/CNK	1.22	1.41	1.31	1.17	0.97	1.13	1.07	1.08	1.27	1.10	1.83	3.03	1.39	1.02	1.06	1.17	1.20	1.86
K2O/Na2O	0.78	0.86	0.95	0.76	0.22	0.59	0.36	0.31	0.48	1.28	3.28	7.83	1.87	1.08	2.60	2.70	2.74	1.62

Table 3c

Representative Trace Element Analyses for Rocks in Willow Wash and Vicinity - New York Mountains

	Garnet-Biotite Gneiss			Misc. Gneiss	Garnet Leuco	Granitic Gneiss	Augen Gneiss		Amphibolites				
	*******	*******	*******	======	#######	======	++++++	++++++	*******	*******	*******	*******	*******
Sample	JW84-18	M88NY-11A	M88NY-39	M88NY-11B	M84	M84	M84	M88	M85	M88	M88	M88	M88
ppm					NY-68B	NY-72	NY-77	NY-03A	NY-10A	NY-02B	NY-08	NY-22	NY-37
Sc	21	10	11	10	0	7	12	9	52	46	39	29	35
Cr	58	56	16	55	1	12	13	12	144	201	73	220	2050
Co	15	9	5	9	0	6	8	9	53	47	55	32	76
Ni		37		46						57	84	78	597
Zn	74.9	93	50	53	2.56	57	51	46	140	134	109	113	106
Rb	101	111	114	197	211	167	94	64		30	12	88	15
Cs	2.13	1.75	1.04	3.42	0.89	2.7	1.18	0.21	0.63	0.71	-0.3	1.43	0.67
Ba	548	279	1320	615	749	672	839	727	317	120	117	550	306
La	53.5	46.1	60.1	39.4	17.3	69.3	66.6	74.9	3.48	1.99	18.3	21.1	12.1
Ce	115	89	118.4	77.3	33.2	160	137	134	7.25	4.9	38.9	43.6	27.6
Nd	45.1	35.4	48.1	31.1	12.9	68.9	54	46	6.76		20.1	20.4	13.9
Sm	8.1	7.89	11	6.73	2.59	15.4	9.09	7.18	2.56	1.45	5.83	5.05	3.04
Eu	1.5	1.37	1.45	1.1	1.31	1.87	1.85	1.76	1.1	0.57	1.72	1.26	0.78
Tb	0.92	1.19	1.58	0.97	0.24	1.41	0.85	0.54	0.67	0.47	0.9	0.64	0.44
Yb	3.37	4.46	5.62	2.02	0.24	1.24	1.25	0.83	2.71	2.63	2.6	2.15	1.17
Lu	0.5	0.61	0.79	0.27	0.03	0.17	0.2	0.13	0.42	0.38	0.38	0.29	0.16
Hf	7.6	6.93	10.2	5.33	1.38	10.9	10.4	9.19	1.7	0.95	3.42	2.57	1.51
Ta	1.27	1.09	1.18	1.14	0.01	0.86	0.45	0.38	0.13	-0.2	1.74	0.51	0.28
Th	17.9	17.1	22.5	15.2	10.2	21.3	9.5	10.8	0.21	-0.2	1.85	3.1	2.57
U	2.53	3.66	5	1.8	0.85	2.3	1.4	0.6		-0.4	0.57	1.46	0.91
Nb	18	16	20	16		24	15	16					
Sr	174	285	440	142	126	108	150	215	172	72	265	530	60
Zr	354	465	515	435	38	450	396	420	62	34	176	126	56
Y	32	54	58	38	13	38	20	14	20	16	22	20	10
Sample/Chondrites													
La	173.1	149.2	194.5	127.5	56.0	224.3	215.5	242.4	11.3	6.4	59.2	68.3	39.2
Ce	142.5	110.3	146.7	95.8	41.1	198.3	169.8	166.0	9.0	6.1	48.2	54.0	34.2
Nd	75.3	59.1	80.3	51.9	21.5	115.0	90.2	76.8	11.3		33.6	34.1	23.2
Sm	41.5	40.5	56.4	34.5	13.3	79.0	46.6	36.8	13.1	7.4	29.9	25.9	15.6
Eu	20.5	18.8	19.9	15.1	17.9	25.6	25.3	24.1	15.1	7.8	23.6	17.3	10.7
Tb	19.6	25.3	33.6	20.6	5.1	30.0	18.1	11.5	14.3	10.0	19.1	13.6	9.4
Yb	16.2	21.4	27.0	9.7	1.2	6.0	6.0	4.0	13.0	12.6	12.5	10.3	5.6

Table 4a

Representative Analyses of Post Ivanpah Orogeny Granitoids

	High-Silica		High K2O/Na2O		Metaluminous						Lower K20/Na2O				
	---	---	+++++	+++++	=====	=====	=====	=====	=====	=====	*********	*********	*********	*********	*********
Sample	M90NY-08	B84NY-76b	M90NY-28	M88NY-13	M90NY-20	M88NY-45	JW84-23	M90NY-74	M90NY-18	M90NY-06	88NY-34B	88NY-28	88NY-25	JW84-19	JW88-107
SiO2	76.00	74.90	73.50	70.80	47.00	55.60	62.20	66.1	67.50	68.10	65.50	66.50	67.80	67.80	70.90
TiO2	0.16	0.08	0.25	0.28	1.76	1.82	1.22	1.2	0.83	1.04	0.66	0.72	0.82	0.49	0.36
Al2O3	12.40	13.60	12.90	14.70	15.10	14.30	14.60	13.3	13.80	12.90	16.90	15.60	14.40	15.70	14.60
Fe2O3	0.51	0.12	0.74	0.55	3.68	4.53	1.52	2.21	2.27	2.09	0.19	0.10	1.73	1.07	0.72
FeO	0.57	0.36	1.33	1.29	8.84	5.43	5.20	3.37	2.78	3.04	3.44	3.58	3.21	2.97	1.45
MnO	0.02	0.01	0.02	0.02	0.18	0.13	0.07	0.08	0.04	0.07	0.02	0.04	0.05	0.04	0.02
MgO	0.28	0.16	0.41	0.35	7.70	2.40	1.43	1.12	1.12	1.02	1.30	0.95	1.00	1.08	0.50
CaO	0.84	1.11	1.04	1.10	8.42	5.74	4.03	3.49	2.53	2.98	3.78	3.06	2.44	2.44	2.24
Na2O	2.59	2.67	2.02	2.60	2.50	1.70	2.73	2.61	2.69	2.49	4.10	3.50	3.10	3.56	3.10
K2O	5.26	5.80	5.90	6.44	0.96	3.66	4.33	4.09	3.97	4.20	2.14	3.16	3.28	3.65	4.14
P2O5	0.06	0.05	0.12	0.12	0.27	1.00	0.39	0.54	0.40	0.43	0.34	0.34	0.20	0.06	0.10
CO2	0.09	0.09	0.20	0.10	0.08	0.12	0.35	0.01	0.02	0.02	0.01	0.23	0.08	0.08	0.29
H2O+	0.42	0.31	0.53	0.62	3.09	1.03	0.58	0.66	0.97	0.61	0.66	0.79	0.58	0.57	0.44
H2O-	0.05	0.07	0.06	0.08	0.23	0.06	0.04	0.08	0.11	0.11	0.05	0.03	0.09	0.07	0.12
Total	99.25	99.33	99.02	99.05	99.81	97.52	98.69	98.86	99.03	99.10	99.09	98.60	98.78	99.58	98.98
Fe2O3T	1.14	0.52	2.20	1.97	13.40	10.50	7.24	5.92	5.33	5.43	3.97	4.04	5.26	4.34	2.31
ppm															
Nd	12		16	16	-10	36	34	38	16	34	18	22	40	24	14
Rb	220	150	210	194	40	110	133	192	230	176	154	180	196	145	146
Sr	110	214	124	186	320	310	223	265	154	270	350	290	168	193	200
Zr	156	88	435	335	94	550	1030	680	630	520	495	1050	1250	675	720
Y	24		28	18	22	88	118	86	34	78	26	58	72	30	46
Ba	510		590	1050	235	1300	1900	1000	600	1100	480	1800	760		920
K2O/Na2O	2.03	2.17	2.92	2.48	0.38	2.15	1.59	1.57	1.48	1.69	0.52	0.90	1.06	1.03	1.34
A/CNK	1.08	1.07	1.11	1.11	0.74	0.83	0.88	0.88	1.04	0.92	1.06	1.06	1.10	1.10	1.07

Table 4b

Representative Trace Element Analyses of Post Ivanpah Orogeny Granitoids

	High-Silica		High K2O/Na2O		Metaluminous						Lower K2O/Na2O				
	---------	---------	+++++	+++++	=====	=====	=====	=====	=====	=====	******	******	******	******	******
Sample	M90NY-08	84NY-76B	M90NY-28	M88NY-13	M90NY-20	M88NY-45	JW84-23	M90NY-74	M90NY-18	M90NY-06	M88NY-34	M88NY-28	M88NY-25	JW84-19	JW88-107
ppm															
Sc	3	1	3	3	26	21	16	15	6	14	6	7	9	10	3
Cr	2	1	3		114	20	16		6	5	35	24	13	13	8
Co	2	1	2	2	57	21	13	9	7	8	10	9	8	8	3
Ni					166										
Zn	21	6	44	34	99	118	63	83	76	88	93	74	81	50	37
Rb	215	160	214	207	45	116	122	192	212	171	202	214	189	166	150
Cs	1.14	1.65	1.26	0.98	0.45	0.72	0.39	2.34	1.41	2.14	3.09	2.26	1.33	3.88	1.56
Ba	501	1300	570	1007	245	1350	2000	999	647	1030	411	1840	690	600	880
La	44.4	22.2	115	95	10.6	96.3	63.6	80.1	132	71.3	35.9	99.4	193	120	183
Ce	91.8	39	243	170	24.1	200	180	199	267	164	65.9	183	362	241	348
Nd	32.1	13.4	93	55	14.5	82.8	92.1	95.3	96.3	76.4	25.2	63.2	119	91.9	124
Sm	6.13	2.52	17.4	9.67	3.91	18.7	20.1	18.1	13.3	16.5	4.75	10.9	22.4	18.2	26.5
Eu	0.86	0.9	1.00	0.91	1.29	3.02	2.83	2.99	1.85	2.24	1.06	1.77	1.32	1.31	1.59
Tb	0.62	0.32	1.11	0.54	0.57	2.27	2.97	2.16	0.86	1.96	0.56	1.04	2.32	1.54	2.75
Yb	1.72	0.32	1.06	0.54	1.94	6.24	7.48	5.85	1.52	5.02	0.52	1.94	2.42	0.53	1.4
Lu	0.25	0.038	0.16		0.29	0.85	1.12	0.82	0.215	0.7	0.07	0.29	0.33	0.076	0.21
Hf	3.71	2.55	8.01	6.2	2.21	13.8	22.2	13.2	11.4	12.7	4.66	11.65	19.1	9.1	15.11
Ta	0.47	0.165	0.38	0.57	0.33	1.73	1.6	3.49	1.92	1.91	1.03	0.71	1.14	1.73	0.6
Th	23.9	11.8	78.9	49.6	0.9	4.4	1.9	6.5	16.7	4.9	7.8	17.2	66.2	74.3	96.4
U	2.3	1.4	3.2	2.7	0.3	0.9	0.8	5.6	2.56	3.7	2.5	1.7	4.3	6	7.4
Nb	12		16	16		36	34	38	16	34	18	22	40	24	14
Sr	110	214	124	186	320	310	223	265	154	270	350	290	168	193	200
Zr	156	88	435	335	94	550	1030	680	630	520	495	1050	1250	675	720
Y	24		28	18	22	88	118	86	34	78	26	58	72	30	46
Sample/Chondrites															
La	143.7	71.8	372.2	307.4	34.3	311.7	205.8	259.2	427.2	230.7	116.2	321.7	624.6	388.3	592.2
Ce	113.8	48.3	301.1	210.7	29.9	247.8	223.0	246.6	330.9	203.2	81.7	226.8	448.6	298.6	431.2
Nd	53.6	22.4	155.3	91.8	24.2	138.2	153.8	159.1	160.8	127.5	42.1	105.5	198.7	153.4	207.0
Sm	31.4	12.9	89.2	49.6	20.1	95.9	103.1	92.8	68.2	84.6	24.4	55.9	114.9	93.3	135.9
Eu	11.8	12.3	13.7	12.5	17.7	41.4	38.8	41.0	25.3	30.7	14.5	24.2	18.1	17.9	21.8
Tb	13.2	6.8	23.6	11.5	12.1	48.3	63.2	46.0	18.3	41.7	11.9	22.1	49.4	32.8	58.5
Yb	8.3	1.5	5.1	2.6	9.3	30.0	36.0	28.1	7.3	24.1	2.5	9.3	11.6	2.4	6.7

Representative Analyses of Metaigneous Rocks - North Providence Mountains

	Granitic Gneisses					Amphibolites		
Sample	M83MH-92	M84MH-58	M84MH-60	JW85-28	JW85-29	M85MP-11	M85MP-12A	M85MP-12B
SiO2	72.80	73.00	67.20	68.00	68.10	51.70	46.70	44.10
TiO2	0.37	0.30	0.81	0.74	0.73	1.09	1.18	2.37
Al2O3	12.30	12.20	13.50	13.40	13.40	14.40	14.40	13.70
Fe2O3	2.19	2.31	2.59	6.16	3.19	3.17	3.14	8.85
FeO	1.48	1.35	3.74	0.45	3.00	7.66	9.24	10.77
MnO	0.02	0.04	0.09	0.09	0.09	0.16	0.31	0.29
MgO	0.37	0.33	1.45	1.22	1.25	6.01	8.39	6.17
CaO	1.30	1.27	2.80	2.81	2.32	11.10	11.30	7.22
Na2O	2.01	2.21	2.31	2.65	2.59	3.08	2.28	2.56
K2O	5.89	5.30	3.05	3.98	4.04	0.54	1.18	2.01
P2O5	0.09	0.13	0.21	0.19	0.19	0.30	0.14	0.30
CO2	0.04	0.02	0.34	0.06	0.05	0.18	0.14	0.15
H2O+	0.40	0.32	1.09	0.62	0.87	1.05	1.46	1.72
H2O-	0.11	0.11	0.14	0.08	0.08	0.09	0.10	0.09
TOTAL	99.37	98.89	99.32	100.45	99.90	100.53	99.96	100.30
ppm								
Rb	197	164	94					
Sr	116	104	128					
Zr	306	349	356					
Y	25	34	50					
Ba	1040	984	807					
A/CNK	1.02	1.04	1.11	0.97	1.04			
K2O/Na2O	2.93	2.40	1.32	1.50	1.56			

Table 5.

Appendix 1, Table 1

Chemistry data for Proterozoic rocks, Optional Stop 2, Day 1.

	amphibolite	amphibolite	biotite gneiss	biotite augen gneiss	biotite augen gneiss	biotite augen gneiss	trondjhemite	trondjhemite	trondjhemite	trondjhemite
	M91IV-102	M91IV-107	M91IV-101	M91IV-105	M91IV-109	M91IV-110	M91IV-103	M91IV-104	M91IV-106	M91IV-108
SiO2	50.3	48.2	75.8	69.5	66.1	64.0	69.2	69.2	68.0	69.9
TiO2	1.02	0.88	0.56	0.55	0.87	0.90	0.18	0.22	0.33	0.18
Al2O3	14.3	13.0	11.8	13.8	14.9	15.4	16.8	16.2	16.4	16.4
Fe2O3	2.72	3.05	0.52	0.96	1.17	1.34	0.65	0.79	0.68	0.46
FeO	8.53	9.32	3.05	2.95	3.95	4.07	1.37	1.35	1.86	1.38
MnO	0.21	0.29	0.05	0.02	0.03	0.04	0.03	0.02	0.03	0.02
MgO	7.87	9.37	1.07	0.87	1.30	1.36	1.25	1.10	1.43	0.98
CaO	10.5	11.4	2.50	2.23	3.45	3.57	4.13	3.71	4.15	3.40
Na2O	2.65	0.71	2.71	2.42	2.96	2.87	4.52	4.58	3.67	4.62
K2O	0.78	0.84	1.07	4.38	2.88	4.47	1.01	1.19	1.95	1.34
P2O5	0.29	0.24	0.13	0.19	0.33	0.34	0.07	0.09	0.20	0.07
LOI	0.54	1.75	0.31	0.96	0.81	0.51	0.47	0.49	0.44	0.37
TOTAL	99.71	99.05	99.57	98.84	98.75	98.87	99.68	98.94	99.14	99.12
K2O/Na2O	0.29	1.18	0.39	1.81	0.97	1.56	0.22	0.26	0.53	0.29
A/CNK	0.59	0.57	1.16	1.08	1.04	0.96	1.05	1.04	1.04	1.08
H2O+	1.34	2.36	0.38	0.75	0.70	0.61	0.44	0.40	0.45	0.41
H2O-	0.07	0.08	0.06	0.21	0.15	0.11	0.08	0.07	0.10	0.10
CO2	0.12	0.41	0.05	0.26	0.39	0.13	0.04	0.14	0.03	0.07
Rb	19.8	44.6	66.9	187	168	162	40.4	46.6	98.0	70.0
Sr	190	<190	239	160	179	227	344	437	517	468
Ba	129	113	234	1210	1590	1920	271	378	444	266
Cs	<0.20	<0.30	1.77	1.34	2.07	0.91	1.75	1.99	2.81	2.34
Rb/Sr	0.10	>0.23	0.28	1.17	0.94	0.71	0.12	0.11	0.19	0.15
Nb	10	14	13	21	25	24	<10	<10	<10	<10
Zr	<110	<210	408	610	890	840	95	100	88	83
Hf	1.88	1.47	9.22	15.4	21.7	19.7	2.34	2.12	2.49	2.24
Y	22	23	24	52	75	84	<10	<10	<10	<10
U	0.98	0.56	3.11	1.84	2.34	<1.00	<0.90	0.76	0.93	<0.90
Th	2.19	1.23	16.1	67.8	17.1	20.1	2.26	3.14	9.37	2.96
Zn	100	131	56.2	65.3	76.0	76.3	31.4	43.0	45.6	41.3
Cu	36	10	15	<10	13	29	<10	<10	36	<10
Ni	98	153	20	<13	<40	<27	16	<11	14	<10
Cr	415	484	47.9	12.4	19.1	23.4	12.8	16.1	19.3	7.3
Co	49.2	53.2	9.35	7.56	11.2	11.9	6.76	7.32	8.35	6.21
Sb	<0.20	<0.08	<0.09	<0.10	<0.10	<0.10	<0.10	<0.10	<0.10	<0.10
Sc	37.6	43.8	8.31	4.02	14.2	13.98	4.73	4.84	4.87	3.95
Ta	0.220	0.217	0.790	0.820	1.12	0.800	0.159	0.163	0.352	0.473
La	9.26	6.57	43.4	196	96.5	134	9.10	9.61	28.2	7.38
Ce	19.9	14.7	83	394	211	274	18.0	17.6	52.1	13.7
Nd	11.3	9.0	35.1	145	103	116	8.2	7.2	19	6.5
Sm	3.05	2.53	6.66	24.7	24.2	23.6	1.63	1.37	3.41	1.11
Eu	0.98	1.00	1.21	1.90	2.21	2.47	0.437	0.412	0.635	0.387
Tb	0.64	0.500	0.735	1.98	2.96	2.64	0.154	0.139	0.308	0.13
Yb	2.46	2.08	2.48	2.86	3.77	5.46	0.48	0.47	0.70	0.39
Lu	0.363	0.316	0.353	0.358	0.428	0.74	0.051	0.058	0.063	0.03